Genome-wide DNA methylome and transcriptome profiling reveals key genes involved in the dysregulation of adipose-stem cells in Crohn's disease

Monfort-Ferré D[a], Boronat-Toscano A[a], Sanchez-Herrero J.F[b], Caro A[c], Menacho M[d], Vañó-Segarra I[a], Martí M[e], Espina B[c], Pluvinet R[b,f], Cabrinety L[d], Abadia C[d], Ejarque M[a], Nuñez-Roa C[a], Maymo-Masip E[a], Sumoy L[b], Vendrell J[a], Fernandez-Veledo S[a], Serena C[a]*

Running title: **Dysregulation of adipose-stem cells in Crohn's disease**

[a]Hospital Universitari de Tarragona Joan XXIII. Institut d´Investigació Sanitària Pere Virgili (IISPV). Universitat Rovira i Virgili, Tarragona, Spain.
[b]High Content Genomics and Bioinformatics, Institut d'Investigació Germans Trias i Pujol, 08916, Badalona, Spain
[c]Colorectal Surgery Unit, Hospital Universitari Joan XXIII, 43007, Tarragona, Spain.
[d]Digestive Unit, Hospital Universitari Joan XXIII, 43007, Tarragona, Spain.
[e]Colorectal Surgery Unit, General Surgery Service, Hospital Valle de Hebron, Universitat Autonoma de Barcelona, 08035, Barcelona, Spain.
[f]Institut d'Investigació contra la Leucemia Josep Carreras (IJC), 08916, Badalona, Spain.

Corresponding author information: Carolina Serena, PhD (ORCID: 0000-0003-2251-0856) (carolina.serena@iispv.cat; carolserena@gmail.com).

Conference presentation: 17th Congress of European Crohn's and Colitis Organisation, ECCO 2022. 16-19 February, online. E-poster. *Journal of Crohn's and Colitis*, Volume 16, Issue Supplement_1, January 2022, Pages i183–i184, https://doi.org/10.1093/ecco-jcc/jjab232.212

keywords: adipose-derived stem cells, DNA methylation, transcriptomics, adipose tissue, creeping fat.

Abstract

Background and Aims Crohn's disease (CD) is characterised by the expansion of mesenteric adipose tissue (MAT), named creeping fat (CF), which seems to be directly related to disease activity. Adipose-stem cells (ASCs) isolated from the CF of patients with CD are extremely pro-inflammatory, which persists during disease remission. We hypothesised that the dysfunctional ASCs in CD accumulate epigenetic modifications triggered by the inflammatory environment that could serve as molecular markers.

Methods Genome-wide DNA methylome and transcriptome profiling were performed in ASCs isolated from MAT adipose-tissue biopsies of patients with active and inactive disease and from non-Crohn's disease patients (non-CD). A validation cohort was used to test the main candidate genes via qPCR in other fat depots and immune cells.

Results We found differences in DNA-methylation and gene expression between ASCs isolated from patients with CD and from non-CD subjects, but we found no differences related to disease activity. Pathway enrichment analysis revealed that oxidative stress and immune response were significantly enriched in active CD and integration analysis identified *MAB21L2*, a cell fate-determining gene, as the most affected gene in CD. Validation analysis confirmed the elevated gene expression of *MAB21L2* in MAT and in adipose tissue macrophages in active CD. We also found a strong association between expression of the calcium channel subunit gene *CACNA1H* and disease remission, as *CACNA1H* expression was higher in ASCs and MAT from patients with inactive CD, and correlates negatively with C-reactive protein in peripheral blood mononuclear cells.

Conclusion We identified a potential gene signature of CD in ASCs obtained from MAT. Integration analysis highlighted two novel genes demonstrating a negative correlation between promoter DNA methylation and transcription: one linked to ASCs in CD (*MAB21L2*) and the other (*CACNA1H*) related to disease remission.

1. Introduction

Inflammatory bowel disease (IBD), which includes ulcerative colitis and Crohn's disease (CD), is a major global health issue affecting ~0.5% of the general population.[1] IBD is associated with a significant economic burden, and the annual direct cost of healthcare in Europe is estimated to be between €4.6 and €5.6 billion, with hospitalisations, surgery, and drugs identified as the main cost factors. It is believed that the indirect cost of IBD, such as lost productivity at work, far outweigh the direct cost.[2] Since the aetiology of IBD is not completely understood, current therapy approaches reduce the clinical manifestations of the disease, but a cure is not yet known.

A hallmark of CD is the occurrence of mesenteric adipose tissue (MAT), commonly referred to as "creeping fat" (CF), which migrates to the inflamed segments of the intestine. It is now appreciated that adipose tissue (AT) is a dynamic and active endocrine organ that, in addition to being an energy storage site, also regulates the immune system and metabolism. Excessive and dysfunctional AT is the cause of many chronic diseases, including metabolic syndrome.[3] AT hyperplasia is triggered by the recruitment and proliferation of AT precursors known as AT-derived mesenchymal stem cells (or ASCs), which leads to an increase in the number of adipocytes.[4,5] ASCs are involved not only in the renewal and maturation of adipocytes, which occurs at a turnover rate of about 10% annually, but they also have immunoregulatory properties that can be modified by the underlying pathological state,[5] including in CD.[6] Single-cell epigenomic techniques have the potential to transform our knowledge of gene regulation and are now becoming mainstream. The epigenome, which includes DNA methylation as a key regulatory process, is heavily influenced by microenvironmental signals in both healthy and pathological contexts. Methylation is a stable modification of genomic DNA that is essential for differentiation processes and for defining tissue-specific transcriptional profiles, but it is also subject to dynamic changes and can be aberrantly regulated in disease states.[6] The accumulation of epigenetic modifications through methylation of specific CpG sites has a key role in chronic diseases.[7,8]

We hypothesised that the inflammatory milieu in active CD induces epigenetic modifications in the DNA methylation profile of ASCs, influencing their anti-inflammatory and regenerative capacity, and that these modifications would remain during CD remission and affect

cell functionality. We tested this hypothesis by first comparing the methylation patterns of ASCs isolated from patients with CD with different clinical activity and from non-CD subjects. We then looked for possible interactions between differentially-methylated DNA sites and the transcriptome profiles of ASCs that might contribute to the aberrant properties of ASCs in CD.

2. Material and methods

2.1. Subjects and study design

Patients with active and inactive CD and non-CD subjects were recruited at the Joan XXIII Hospital (Tarragona, Spain) and the Vall d'Hebron University Hospital (Barcelona, Spain), and all gave their informed consent. The study was conducted in accordance with the principles of the Declaration of Helsinki and was approved by the ethics and research committees of the respective hospitals (references CEIM 177/2018; CEIM 41p/2015; PR(CS)383/2021). Patients were classified into in relapse (active) and in remission (inactive) following criteria of the Crohn's Disease Activity Index (CDAI) and based on clinical and biological parameters such as high-sensitivity C-reactive protein (hsCRP). Endoscopic evaluation was performed in 75% of patients, with complete concordance with the clinical classification obtained by CDAI.[9,10] Non-CD were recruited from subjects undergoing non-acute surgical interventions, such as cholecystectomy, while inactive CD were recruited from subjects undergoing scheduled routine surgery for intestinal transit reconstruction. Patients with active CD were recruited from those undergoing surgery for symptomatic complications. All samples were aseptically collected and (when appropriate) were obtained before bowel opening or resection to avoid possible contamination. Clinical data, anthropometric, demographic, and biochemical variables of the cohort are shown in Table 1.

For active CD patients, we have obtained MAT from two origins: unhealthy MAT (CF) or healthy MAT (hMAT). CF adipose tissue (n=7) was taken from the area of MAT adjacent to the specimen to the bowel that was resected. The sample was taken with scissors to avoid lesions of the sample and from the adipose tissue closest to the bowel. Healthy MAT (n=7) was taken from another part of the MAT, generally close to the distal jejunum or the proximal ileum (any

area free of disease in the complementary tests performed prior surgery). We took a small sample, approximately 1-2 cm, of the MAT from an area that macroscopically appeared healthy.

For inactive CD patients (n=7) and non-CD patients (n=7), healthy MAT samples were acquired from MAT, usually near the small bowel, following the same meticulous sampling protocol. A small sample, approximately 1-2 cm in size, was extracted from an area macroscopically deemed healthy.

We also obtained some biopsies from subcutaneous adipose tissue (SAT) of the three groups studied. The samples were collected from the incision site made for the extraction of the surgical specimen. It is usually a small laparotomy in the midline.

The summary of cell types isolated, and tissues used in the study is described in Table 2.

2.2. Isolation of ASCs

Tissue samples (hMAT or CF) were first washed with PBS to remove traces of blood, and when needed, the areas damaged by the surgery were removed with a scalpel. Samples were then treated with 0.1% collagenase and 1% BSA in PBS for 90 minutes at 37°C under gentle agitation. The digested samples were centrifuged at 300 × *g* at 24°C for 5 minutes for phase separation, with the mature adipocytes at the top and the vascular stromal component in the pellet, consisting mainly of stem cells, macrophages, endothelial cells and blood cells. Mature adipocytes were carefully removed and stored, and another wash and centrifugation cycle was performed to isolate the pellet. Specifically, the centrifuged pellet was resuspended in DG maintenance medium (DMEM / F12 in 10% foetal bovine serum) and cells were seeded in a T75 ask and allowed to grow for 7 days at 37°C to 90% confluence and then harvested with trypsin-EDTA, resulting in a primary culture at passage 0.[11] MAT-derived macrophages (ATMs) were also isolated from the stromal vascular fraction of AT biopsies as described.[12–16]

2.3. ASC immunophenotyping

Cells (2×10^5) were incubated with a panel of primary antibodies (described in supplemental table S1).[17] After isolation, the minimal functional and quantitative criteria, established by the

International Society of Cell Therapy and the International Federation for Adipose Therapeutics and Science, were confirmed by flow cytometry.[16–18] All experiments were performed in cells at passage 3.

2.4. DNA methylation profiling

Genomic DNA was extracted from cells using the NucleoSpin® Tissue Kit (Macherery-Nagel GmbH, Dueren, Germany). Global DNA methylation profiles were determined with the Human-MethylationEPICBeadChip Infinium assay (Illumina Inc., San Diego, CA), developed to quantitatively assay over 850,000 methylation sites across the genome at single-nucleotide resolution. Hybridised BeadChips were imaged on an Illumina HiScan system (Supplementary S2). We used the Methylation Atlas Deconvolution standalone program for cell type deconvolution [19,20] to evaluate whether cell admixture contributes significantly to the results in our cell population Our findings revealed predominant matches of our samples with adipocytes, cervix uteri, vascular endothelium, left atrium, breast, pancreas, and kidney (Supplementary figure S1). The heatmap illustrates similar DNA methylation profiles across these reference cell types. Importantly, it should be noted that DNA methylation data for ASCs are not currently incorporated into this reference atlas. Nevertheless, our DNA methylation data align with related cell types such as adipocytes. Methylation data have been deposited in the GEO database with the accession code GSE217124.

2.5. Analysis of differentially-methylated loci

All pre-processing and statistical data treatment was performed using the R statistical programming environment (version 4.2.0; R core team, 2022). DNA methylation raw data (.idat files) were read using the Bioconductor package RnBeads (v2.14) and the annotation package RnBeads.hg19 (v1.28).[21–23] Gender and hospital of each patient were used as covariates in the linear model. Furthermore, an additional analysis was conducted, incorporating smoking status and CRP levels as covariates to test the robustness of the methylation results. Given the non-random allocation of our samples onto the methylation chips (as detailed in Supplementary Table

S2), we recognized the potential for introducing uncontrollable batch effects. Consequently, to assess and mitigate the impact of such effects, we used ComBat, implemented in the sva R package, [24–26] to remove possible batch effects derived from subarray position (sentrix position) and slide (sentrix ID) due to the non-random placement of samples on the beadarrays. A total of 18.56% of the probes were discarded as they were identified as SNP-enriched probes; they contained low detection p-values or standard deviations; they were beyond the GpG context or within sex chromosomes; or they were included in a blacklist as putative error-prone probes (Product Change Notification, PCN2019-019). The beta-mixture quantile normalisation (bmiq) algorithm was used to normalise probe intensities.[27] CpG methylation levels were calculated as M-values and β-values. Differentially methylated positions (DMPs) were located through linear regression using dmpFinder[28] and differentially methylated regions (DMRs) were identified using bumphunter,[29] both functions within the minfi library package. DMPs and DMRs were calculated using default settings, with the latter including the smoothing option, 100 permutations and a mean difference threshold between groups of 0.2. We also filtered for at least three consecutive CpGs within a DMR. [30,31] The R variance partitioning package[32] was used with a linear model incorporating fixed variables (Crohn's disease, CRP, smoking, hospital, and gender) to assess the contribution of each variable to methylation changes.

2.6. Transcriptome analysis

RNA was extracted using TRIzol reagent and further purified/DNase-treated with the RNeasy Mini Kit (Qiagen, Hilden, Germany). RNA sequencing libraries were prepared using the TruSeq Stranded mRNA Library Prep Kit (Illumina) with 200 ng of total RNA used as input. Libraries were qualified with Bioanalyzer DNA 1000 chips (Agilent, Santa Clara, CA) and quantified by qPCR using the KAPA Library Quantification Kit KK4835 (Roche, Basel, Switzerland) prior to sequencing. Libraries were sequenced 1x50 to at least 24 million reads per sample on the Illumina HiSeq2500 platform with v4 SBS reagents.

FastQC (version 0.11.9; BaseSpace Labs, Illumina) and MultiQC[33] were used to evaluate the quality of raw-read fastq data files. We applied quality trimming using trimmomatic[34] (v0.30).

Reads were mapped against the *Homo sapiens* reference genome (Ensembl release 78, Homo_sapiens.GRCh38.dna.primary_assembly) using STAR software (v2.5.2)[35] and were assigned to genes using FeatureCounts from subread software (v. 2.8.2). Differential expression analysis was performed using the DESeq2[36] package with the Wald test and an Approximate Posterior Estimation for the Generalised Linear Model (apeglm)[37] approach to check the differentially expressed genes (DEGs) between conditions. Gender and age of each patient were used as covariates in the model. Volcano plots were produced using the EnhancedVolcano[38] R package. All RNA sequencing data have been uploaded to Gene Expression Omnibus (GEO) with the accession number GSE217163.

2.7. Gene set enrichment analysis and visualisation

We performed gene set enrichment analysis (GSEA) using DEGs lists ranked by $\log_2$-fold change or signed $\log_{10}$ p-value against the Molecular Signatures Database (MSigDB) gene set collections.[39,40] Analysis was done using R and the fgsea[41] package and visualisations were generated using the ggplot2 package.

2.8. Integration analysis

DNA methylation and gene expression results were integrated for each gene. We used annotation for each methylation probe (at promoter, CpG island, and gene level), assigning a gene or associated gene symbol to match with gene-level transcriptomic data. Focusing only on the set of DEGs, we retrieved all the probes associated for each region and we correlated for each set of probes the methylation and the expression values of a gene. We retained those genes with significant methylation-transcription correlation ($p<0.05$).

2.9. Isolation of peripheral blood mononuclear cells

Peripheral blood mononuclear cells (PBMCs) were isolated with Pancoll human MSL (Pan Biotech GmbH, Aidenbach, Germany). Pellets were frozen and stored at -80ªC until RNA

extraction. Clinical and demographic data of donors are described in online Supplementary Table S3.

2.10. RNA extraction

For validation of candidate's genes (integrative study of significant DMPs and DEGs) in other tissues or cells by RT-PCR, the RNA was extracted from 200 mg of MAT/SAT, or 100,000 cells of ATMs, mature adipocytes and ASCs using the TriPure Isolation Reagent (Roche, Basel, Switzerland). RNA concentration was determined by absorbance at 260 nm, and purity was estimated with a Nanodrop spectrophotometer (Nanodrop Technologies Inc., Wilmington, DE). cDNA was synthesised using SuperScript II reverse transcriptase and random hexamer primers (Invitrogen Life Technologies, Darmstadt, Germany).

2.11. Real-time quantitative PCR

Quantitative gene expression of *MAB21L2* (Hs00740710_s1) and *CACNA1H* (Hs01103527_m1) was evaluated by quantitative real-time PCR (qPCR) on a 7900HT Fast Real-Time PCR System using TaqMan Gene Expression Assays (Applied Biosystems). Results were calculated using the comparative threshold cycle (Ct) method ($2^{-\Delta\Delta Ct}$) normalised to the expression of the housekeeping gene *18S* (Hs03928985_g1) and expressed relative to the non-CD condition. Two technical duplicates were performed for each biological replicate.

2.12. Statistical analysis

Statistical analyses were performed using multiple tools. For *omics* analysis, we used the R statistical programming language and several packages as described and ggplot2[42] for visualisation. We also used the Statistical Package for the Social Sciences software, version 15 (SPSS, Chicago, IL). For clinical and anthropometrical variables, normally distributed data are expressed as mean ± SD; for variables with no Gaussian distribution, values are expressed as median (25th–75th quartiles). Student's t-test with Bonferroni adjustment was used to compare the mean value of normally distributed continuous variables. For variables that did not have a

Gaussian distribution, we used the Kruskal–Wallis test with *post hoc* Dunn's multiple comparisons test. To analyse the differences in nominal variables between groups, we used the $\chi 2$ test. Pearson's correlation coefficient with Bonferroni adjustment was used to analyse the relationship between parameters. For *in vitro* data, experimental results are presented as mean ± SEM. Comparisons among the three groups were performed using the non-parametric Krustal-Wallis test. Data visualisations were created with GraphPad Prism v6 (Graphpad Software Inc., San Diego, CA).

3. Results

3.1.CD per se but not clinical activity or disease location influences DNA methylation and gene expression of ASCs

We analysed the genome-wide DNA methylation and mRNA expression profiles of ASCs from non-CD patients (hMAT n=7) and from patients with inactive (hMAT n=7) and active (CF n=7 and hMAT n=7) CD patients. ASCs were obtained from healthy hMAT from all three groups and from CF in the active CD group. To note, three samples did not pass the quality control of DNA methylation. Specifically, one sample of CF of active CD patients and two samples of hMAT of inactive CD patients. We first examined DNA methylation data to identify DMRs and DMPs. For the former, we used ≥3CpGs (3 or more adjacent positions within the same gene), which yielded 70 DMRs between ASCs from non-CD and active CD and 67 DMRs between non-CD and inactive CD. Furthermore, 9 DMRs were detected when comparing inactive CD with active CD. For the analysis of DMPs we used as cutoffs in the analysis a mean difference in $\beta > 0.2$ and an adjusted p-value <0.05, which revealed 6501 DMPs between ASCs from non-CD and active CD, and 628 DMPs between non-CD and inactive CD. Intriguingly, no significant DMPs were found between active CD and inactive CD groups (figure 1A). For RNAseq analysis we used as cutoffs in the analysis of DEGs an absolute fold-change (FC) >1.2 and an adjusted p-value <0.05. Results yielded 86 DEGs between ASCs from non-CD and active CD, 60 DEGs between non-CD and inactive CD and only 3 DEGs between active and inactive CD (figure 1A). Finally, we performed integration analysis using a linear regression model considering all DEGs and the methylation

probes within the associated region (gene, promoter and CpG island), which yielded 20 significant correlations between non-CD and active CD, 9 correlations between non-CD and inactive CD and 6 correlations between active CD and inactive CD; an example of a strong correlation found in *MAB21L2* is shown in figure 1A.

Then, we used principal component analysis (PCA) to explore relationships among the different groups and applied the first two principal components (PC1 and PC2) of the DNA methylation and RNAseq data. The DNA methylation data showed that the three groups differed in groupings, but no differences were observed between ASCs from the CF and hMAT tissues of patients with active CD (figure 1B). Moreover, there was no clear separation between the three groups in PCA plots based on RNAseq data, consistent with the limited number of DEGs (figure 1B). We next performed heatmap visualisation of the top 50 significant DMPs and DEGs, finding that non-CD-ASCs and CD-ASCs could be clearly discriminated. Independently, DNA methylation or RNAseq profiles could not be used to discriminate between active and inactive CD groups, indicating that the major changes occurring in ASCs were maintained in disease remission (figure 1C).

3.2. CD induces permanent changes in the DNA methylome of ASCs

To specifically evaluate the methylation patterns and preferential genome locations, we segmented all significant DMPs with an adjusted p-value <0.05 into the following five categories according to the Illumina annotations: island, north shore, south shelf, open sea and south shore (figure 2A, right panel). Results showed that the DMPs distribution was mainly located in open sea regions (75%). The distribution of the Illumina EPIC array probes is shown in figure 2A (left panel).

Summarized differential methylation results between CD subjects and non-CD controls in promoter regions is depicted in the volcano plot (figure 2B). Notably, the MAB21L2 gene was hypomethylated in the promoters of CD subjects. Other genes such as RNU6-781P, AXL4 and RN7SL148P were also hypomethylated in the promoters of CD subjects. In contrast, HOXD4,

MIR10B, HTR3B, KCNK2, MIR3117 and COX5AP2 displayed hypermethylation in the promoters of CD subjects.

We used the minfi function bumphunter to locate DMRs using default settings and the smoothing option.[43] We found 95 regions located near known annotated genes. Filtering for those genes with ≥3 significant DMRs in promoter regions and a p-value cutoff of <0.05, we obtained 21 DMRs between non-CD and active CD, 18 DMRs between non-CD and inactive CD and only 5 DMRs between active and inactive CD (supplemental table S4). Notably, MAB21L2 exhibited 9 significant DMRs in both the active CD versus non-CD group and inactive CD versus non-CD group comparisons (figure 2C). Furthermore, to assess the influence of various variables on the primary candidate gene identified in the methylation study, MAB21L2, we employed the Variance Partition R package, applying a linear model with fixed variables [32]. Our analysis revealed that CD status accounted for 60% of the observed variance in MAB21L2 promoter methylation levels, with other variables such as smoking, CRP, hospital, or gender collectively explaining less than 40% of the variance (figure 2D).

Finally, we used ComBat to adjust for systematic variation introduced by different experimental batches, ensuring comparability across batches. Our analysis indicated that the application of ComBat did not yield significant changes in the primary DMPs identified. Moreover, even after adjusting for other covariates known to influence methylation, such as smoking or CRP (Supplementary figure S2), the primary candidate genes identified in this study remained consistent. Of particular significance is the observation that the CRP variable independently exhibits an augmentation in differentially methylated promoters when comparing subjects with CD to those without (non-CD) (figure S2, C). This phenomenon is likely attributed to the notably robust correlation between the presence of CD and CRP levels, serving as a biomarker for disease activity. Consequently, when juxtaposing CD and non-CD subjects, the elevated CRP levels in CD subjects contribute to the emergence of false positives.

3.3. Transcriptomic profiling of ASCs reveals the up-regulation of immune-response genes in CD

The significant differential gene expression (adjusted p-value >0.05) overlaps for the three pairwise comparisons between the different groups is shown in figure 3A. The DEGs of active and inactive CD showed divergent gene expression relative to non-CD (86 and 60 DEGs respectively), with only four genes overlapping between the two comparisons (*MAB21L2, NKX2-3, DBP* and *PDK4*). Notably, only four genes showed significantly different expression between the CD groups with different activity, suggesting that remission of the disease does not restore the gene expression of ASCs. *NHS* was differentially expressed both in non-CD *versus* active CD and inactive *versus* active CD comparisons, whereas *NAPRT* was differentially expressed in the comparison between non-CD and inactive CD and between inactive and active CD.

A volcano plot depicting statistical significance (as $-\log_{10}$ p-value) versus $\log_2$ fold-change between non-CD and active CD is presented in figure 3B, left panel. DEGs with most significant differences are highlighted in red (adjusted p-value <0.05). Results showed that *NKX2-3, HAND1* and *MAB21L2* were up-regulated in the active CD group (Log_2 fold-change >4) with *NKX2-3* as the most significant DEG between the active CD and non-CD groups. Notably, *NKX2-3* has been linked to IBD pathogenesis.[44] Contrastingly, *PRELP, CCN5, KRT16, VIT, TGBR3* and *ADRA2B* were significantly up-regulated in the non-CD group (Log_2 fold-change < -4). Some of these genes are essential for the structural and functional integrity.[45–47]

We next used GSEA to assess the biological pathways differentially regulated between conditions (figure 3B, right panel). We found seven up-regulated pathways in ASCs isolated from active CD, of which the most significant were the following: *activation of reactive ENOS, Weigel oxidative stress by HNE and H_2O_2* and *Reactome co-stimulation by the CD28 family*. All of these pathways affect oxidative stress and the immune system.[48] Surprisingly, expression of *NKX2-3* and *MAB21L2* was higher in ASCs from inactive CD than from non-CD (Log_2 fold-change >4), and both genes were also significantly elevated in active CD (figure 3C, left panel). However, only *the reactome respiratory electron transport* pathway was found enriched among DEGs upregulated in the inactive CD group relative to non-CD (figure 3C, left panel). Finally, we failed to find any significant DEGs between ASCs from active and inactive CD groups (figure 3D), suggesting that ASC of active and inactive CD have a similar profile.

3.4. Integration of DNA methylation and gene expression identifies *MAB21L2* as a potential marker of CD

Integration of DNA-methylation and RNAseq data pointed to *MAB21L2* as a potential key gene involved in CD pathogenesis. We found low DNA methylation in the promoter of the *MAB21L2,* which agrees with its elevated gene expression in both active and inactive CD. We observed a significant overall negative correlation between methylation and expression both in active ($p = 6.8\times10^{-6}$) (figure 4A) and inactive ($p = 4.5\times10^{-6}$) CD (figure 4B) relative to the non-CD group. There was also a significant negative correlation within each CD group, suggesting a gradation in patient expression levels directly dependent on promoter methylation status in the *MAB21L2* CpG sites evaluated.

To validate the results of the integrative study we used qPCR to examine *MAB21L2* gene expression, which confirmed the significantly elevated expression of *MAB21L2* in ASCs isolated from active and inactive CD groups relative to the non-CD group (n=7/each group) (figure 4C). We next questioned whether *MAB21L2* was also expressed in adipose depots, MAT or SAT, with results showing that *MAB21L2* expression was significantly higher in MAT of active CD patients compare to SAT of active patients and compare to MAT of non-CD subjects (figure 4D). We subsequently focused on active CD to investigate the expression of *MAB21L2* in the cellular components of adipose tissue (mature adipocytes and ATMs). *MAB21L2* expression was significantly higher in ATMs and ASCs than in mature adipocytes, and expression was significantly higher in ASCs than in ATMs (figure 4E). Finally, we studied the expression of *MAB21L2* in PBMCs between the three groups. Results indicated a non-significant trend for higher expression of *MAB21L2* in CD groups (active and inactive) (figure 4F). *MAB21L2* expression also positively correlated with the abundance of the inflammatory marker hsCRP in serum (figure 4G). Finally, we found that higher *MAB21L2* expression was associated with higher levels of hsCRP ($p=0.0077$), confirming that elevated *MAB21L2* expression is associated with CD.

3.5. *CACNA1H* is potentially important in CD remission

Differential integration analysis of ASCs revealed a significant correlation between RNA levels and promoter DNA methylation in the gene coding for calcium voltage-gated channel subunit alpha 1H (*CACNA1H*). ASCs isolated from patients with inactive CD showed low DNA-methylation in the *CACNA1H* promoter, which negatively correlated with an elevated gene expression as compared with the non-CD group (p=0.034) (figure 5A) and with the active group (p=0.032) (figure 5B). No significant correlation was found in a similar assessment between non-CD and active CD, indicating that *CACNA1H* is linked to the remission phase of the disease.

We validated the expression of *CACNA1H* gene by qPCR in ASCs isolated from non-CD and from patients with active and inactive CD (n=7/per group). The gene expression of *CACNA1H* was significantly higher in ASCs isolated from the inactive group than from non-CD and active CD groups (figure 5C). We thus focused on ASCs isolated from the inactive CD group, and we studied the *CACNA1H* gene expression in the different tissues and cellular components of AT. *CACNA1H* expression was significantly higher in hMAT than on SAT in CD subjects (figure 5D). Notably, *CACNA1H* expression was significantly higher in ASCs than in AT components (MAT and mature adipocytes) and was also significantly greater in hMAT than in mature adipocytes (figure 5E). Finally, we examined the expression of *CACNA1H* in PBMCs in all three groups, finding significantly higher expression in PBMCs from inactive CD than from active CD, and significantly lower expression in PBMCs from active CD than from non-CD (figure 5F). Notably, we observed a significant negative correlation between *CACNA1H* expression and hsCRP levels in serum (p=0.0222) (figure 5G), suggesting that *CACNA1H* expression is associated with disease remission.

4. Discussion

In the context of CD, the mesentery and MAT play pivotal roles in disease pathogenesis and progression. The mesentery, a crucial anatomical structure, serves as a connective tissue framework that supports and anchors the intestines within the abdominal cavity. It facilitates intestinal mobility and provides a conduit for blood vessels, lymphatics, and nerves essential for

intestinal function. Conversely, MAT, the fat tissue surrounding the mesentery, is emerging as a dynamic contributor to the inflammatory milieu observed in CD. This visceral fat depot serves not only as an energy reservoir but also as a source of pro-inflammatory cytokines and adipokines. Growing evidence suggests that alterations in MAT composition and function may exacerbate local inflammation and contribute to disease pathophysiology. In this sense, ASCs within MAT, are a significant source of immune-competent cells. Indeed, ASCs isolated from patients with CD exhibit an aberrant functional profile with enhanced proliferative, invasive, inflammatory and phagocytic capacities,[18] and the inflammatory milieu of MAT in CD is associated with ASC dysregulation.[18] Hyper-inflammation is also linked to bacterial translocation, which likely drives the formation of CF in active CD.[49–51] It is highly possible that the inflammatory microenvironment triggers changes in DNA methylation and gene expression in ASCs from patients with CD. Our results suggest that changes in ASCs are permanent and sustained even when the disease is in remission.

Here, we report differences in the genome-wide DNA methylome and transcriptome between ASCs from non-CD and from patients with CD with different clinical activity. Our analysis highlighted *MAB21L2* as the most significantly altered gene in ASCs from patients with CD compared to non-CD subjects. *MAB21L2* forms part of the transforming growth factor beta-1 (TGFβ-1) signalling cascade, and is antagonised by TGFβ-1, which inhibits its activation. TGFβ-1 has been shown to be dysregulated in ASCs isolated from patients with IBD also has immunosuppressive functions in healthy cells.[18,52] A previous study in murine immune cells (T cells and dendritic cells) showed that TGFβ-1 down-regulation leads to spontaneous colitis.[53] In agreement, ASCs isolated from patients with CD show decreased expression of *TGFβ*[13] and we found elevated expression of *MAB21L2*. The dysregulation of TGFβ signalling in CD-associated ASCs could be implicated in the increased expression of *MAB21L2*, making this gene a possible target in CD. Furthermore, MAB21L2 overexpression has been associated with a higher risk of recurrence in colorectal cancer patients.[54] Further investigations to determine whether MAB21L2 expression predicts postsurgical recurrence in CD subjects would be valuable.

458 In an earlier study, we found no differences in DNA methylation profiles relative to CD
459 clinical activity in ASCs isolated from SAT.[55] Consistent with this, the present study found only
460 two distinct groups from DMP and DEG analysis: ASCs from non-CD subjects and ASCs from
461 patients with CD. There was no clear distinction between ASCs from patients with active or
462 inactive disease. Overall, these analyses support our earlier findings that ASCs isolated from
463 patients with inactive disease remain dysregulated. Notably, no differences were observed when
464 comparing the various tissues in patients with active CD (CF versus healthy MAT), suggesting
465 that ASCs isolated from both healthy and unhealthy origins within the MAT are impaired in CD
466 patients.

467 Promoter DNA methylation is related to gene transcription, with high DNA methylation
468 at promoter regions associated with lower gene expression and *vice versa*.[56] The epigenetic study
469 highlights that MIR10B was hypermethylated in the promoter of ASCs from CD subjects.
470 Notably, MIR10B has been previously found hypermethylated and downregulated in different
471 cancers and risk of carotid atherosclerosis [57–62] and it has been claimed as a novel tumor
472 suppressor and is partially silenced by DNA hypermethylation in gastric cancer. In contrast,
473 MAB21L2 was hypomethylated in promoters of CD patients, with 9 significant DMPs and 9
474 significant DMRs (Suplemmentary Table S4 and Suplemmentary File S1). It is noteworthy that
475 our study revealed a distinctive hypomethylation pattern within the promoter region of ALX4 in
476 individuals with CD compared to non-CD subjects. This finding aligns intriguingly with
477 observations in hepatocellular carcinoma (HCC), the most prevalent form of liver cancer, where
478 a similar hypomethylation phenomenon has observed. Unlike the prevalent hypermethylation
479 observed in numerous other cancer types like breast and lung cancer, this hypomethylation of
480 ALX4 is associated with its role as a tumor suppressor, suppressing processes like epithelial-
481 mesenchymal transition (EMT), migration, and invasion of cancer cells, suggesting therapeutic
482 potential.[63,64]

483 It is known that environmental factors such as smoking or the inflammatory environment
484 that accounts for CD also affect the methylation pattern of ASCs.[16,55] Therefore, it was crucial to
485 investigate whether covariates such as smoking or CRP levels had an impact on the key candidate

genes identified in our study. While we observed alterations in the methylome of the samples associated with these covariates, it is noteworthy that the primary candidate genes remained significant even after adjusting for these covariates in our analysis.

Examination of DMPs hyper- and hypomethylated in promoter regions revealed similar genes between ASCs from different clinical CD activity, further suggesting that dysregulation of ASCs is maintained in remission of the disease.

In patients with CD, notable alterations in methylation patterns were observed in peripheral blood methylation studies, which were consistent with those observed in ASCs in our study. Specifically, genes such as HLA, ZBTB, TMEM, KCNAB2, and MYOC exhibited consistent methylation changes across both sample types. Specifically, analysis of DMRs outlined in supplementary Table S2, highlighted modifications in methylation levels within the HLA gene, previously associated with immunoregulation and implicated in CD pathogenesis.[65,66] Furthermore, examination of DMPs, included in the Supplementary File F1 revealed consistent variations in methylation patterns, particularly within the ZBTB, TMEM, KCNAB2, and MYOC. Notably, hypermethylation of the KCNAB2 promoter region was observed in both ASCs and peripheral blood DNAm studies, reinforcing its potential significance in the context of CD pathogenesis. These findings underscore the importance of our study in elucidating shared DNA methylation changes across different tissues and emphasize the significance of investigating ASC-specific methylation patterns in understanding CD mechanisms. [67,68]

Transcriptomic analysis revealed a significantly higher expression of *NKX2-3* (NK2 homeobox 3) in ASCs isolated from patients with CD. NKX2-3 has previously been associated with IBD risk and plays an important role in IBD pathogenesis,[48,69] and a meta-analysis of over 35,000 subjects demonstrated an association between genetic variants of *NKX2-3* and CD susceptibility.[44] The elevated expression of *NKX2-3* in ASCs isolated from patients with both active and inactive CD again indicates that ASCs continue to express inflammatory and disease-associated genes even when the disease is in remission. On the contrary, our results show that *TGFBR3* expression is significantly decreased in CF ASCs from patients with CD. In this context,

514 recently Qian and colleagues evidenced that low *TGFBR3* expression has been linked to fibrosis
515 activation in CF-ASCs from patients with CD. [70]

516 Intriguingly, our integration analysis also revealed *CACNA1H* as one of the most
517 significantly increased genes in the remission state of the disease. CACNA1H is involved in the
518 pathophysiology of visceral chronic discomfort and pain associated with irritable bowel syndrome
519 in murine models.[71,72] Picard and colleagues demonstrated that the elevated expression of
520 *CACNA1H* in a murine model of colonic hypervisibility is associated with local low-grade
521 inflammation,[73] which along with abdominal pain is a common feature in irritable bowel disease
522 and in IBD during remission.[74] The elevated expression of *CACNA1H* in inactive CD might be a
523 potential biological marker to determine disease activity in patients, although further studies are
524 needed to explore this.

525 This study has some limitations that warrant discussion. The variability/heterogeneity
526 between samples might add a layer of complexity when interpreting results. For instance, the
527 therapies that patients in our study are on might affect DNA methylation and/or gene transcription
528 in the ASCs. In this regard, however, we did exclude patients treated with biologicals and we
529 have included approximately 50% of patients treated with thiopurines in both active and inactive
530 CD groups, to minimise the effects produced only by the treatments. As another limitation to our
531 study, we acknowledge that the total number of patients included is relatively low and hence some
532 of the analyses performed might be underpowered. Although it would be more valuable to
533 perform paired statistics on the same active CD subject, we were unable to obtain samples from
534 hMAT and unhealthy MAT (CF) of the same patient, which is also another limitation of the study.
535 However, to the best of our knowledge, this is the first and largest study applying a multi-omics
536 profiling approach to ASCs isolated from patients with active and inactive CD. The fact that the
537 location of MAT (CF *versus* hMAT) was studied also represents an important strength.

538 In conclusion, our study underscores that clinical findings alone may not adequately
539 demonstrate remission in CD. We highlight the significant role of ASCs in CD pathology. These
540 cells, influenced by the inflammatory milieu, undergo alterations in DNA methylation and
541 subsequent changes in gene expression, persisting even during disease remission.

Funding

This study was supported by a grant from the European Crohn's and Colitis Organisation (ECCO grant 2019 to CS) and by Fundació La Marató de TV3 (PV170125 to SF-V). This work was also supported by Instituto de Salud Carlos III (ISCIII) (PI18/00037 to CS and PI17/01503 and PI20/00338 to JV), co-funded by the European Union. CS acknowledges support from the "Ramón y Cajal' program from the Ministerio de Educación y Ciencia (RYC2013-13186), co-financed by the ERDF. D.M-F acknowledges support from PERIS-PFI-Salut SLT01720000021. A.B-T acknowledges support from PI-AGAUR 2022-B00577. I.V. acknowledges support from INVESTIGO-AGAUR (100036TC2). JFSH was a beneficiary of a contract partially funded by ISCIII through the Acción Estratégica en Salud 2018 (co-funded by the ERDF/European Social Fund; "A way to make Europe"/"Investing in your future") CA18/00019 (contrato de técnico bioinformático de apoyo a la investigación en los IIS acreditados de IIS). The Spanish Biomedical Research Center in Diabetes and Associated Metabolic Disorders (CIBERDEM) (CB07708/0012) is an initiative of the Instituto de Salud Carlos III. Both SF-V and JV acknowledge support from the Agency for Management of University Research Grants of the Generalitat de Catalunya (2021 SGR 01409, 2021 SGR 00829).

Conflict of interest

The authors have no conflicts of interest to declare.

Data availability

The assession number for DNA methylation and RNAseq data reported in this paper is GSE217164. The other datasets generated during and/or analysed during the current study are available from the corresponding author on reasonable request.

Acknowledgements

We wish to particularly acknowledge the patients and the BioBank IISPV (PT17/0015/0029) integrated in the Spanish National Biobanks Network for its collaboration. We thank Dr. Kenneth McCreath for helpful comments on the manuscript. The High Content Genomics and Bioinformatics of the IGTP provided resources as a service for sample quality control, methylation profiling, RNAseq library preparation, and bioinformatic data analysis. We thank Dave Rojas for support in covariate adjusted model assessment and variance partitioning analysis. We wish to thank the Genomics Unit of the Centre for Genomic Regulation for excellent technical services in next generation sequencing.

Author contributions

D.M-F., A.B-T., M.E., C.N-R., E.M-M., I.V-S. performed the experiments. A.C., M.M., M.Ma., B.E., L.C. and C.A. and carried out part of the study population selection and human sample processing. R.P and L.S performed the genomic assays, J.F.S.H. performed bioinformatic data analysis. J.F.S.H. and L.S contributed to the discussion and reviewed the manuscript. D.M-F., M.E., S. F-V., J.V. and C.S. conceived the study and discussed data. D.M-F and C.S. wrote the manuscript. C.S. is the guarantor of this work.

Ethics approval

This study was approved by the ethics committee of the University Hospital Joan XXIII (CEIM 080/2021, CEIM177/2018, CEIM 41p/2015) and Hospital Vall d'Hebrón PR(CS)383/2021.

References

1. Kaplan GG. The global burden of IBD: From 2015 to 2025. *Nat Rev Gastroenterol Hepatol* 2015;**12**(12):720–7. Doi: 10.1038/nrgastro.2015.150.
2. Jesús Gómez-Gómez G., Masedo Á., Yela C., Del Pilar Martínez-Montiel M., Casís B. Current stage in inflammatory bowel disease: What is next? 1128:40. Doi: 10.3748/wjg.v21.i40.11282.
3. Paniagua JA. Nutrition, insulin resistance and dysfunctional adipose tissue determine the different components of metabolic syndrome. *World J Diabetes* 2016;**7**(19):483. Doi: 10.4239/WJD.V7.I19.483.
4. Gonçalves P., Magro F., Martel F. Metabolic Inflammation in Inflammatory Bowel Disease: Crosstalk Between Adipose Tissue and Bowel. *Inflamm Bowel Dis* 2015;**21**(2):453–67. Doi: 10.1097/mib.0000000000000209.

5. Zulian A., Cancello R., Ruocco C., Gentilini D., Di Blasio AM., Danelli P., et al. Differences in Visceral Fat and Fat Bacterial Colonization between Ulcerative Colitis and Crohn's Disease. An In Vivo and In Vitro Study. *PLoS One* 2013;**8**(10). Doi: 10.1371/journal.pone.0078495.
6. Feinberg AP. Phenotypic plasticity and the epigenetics of human disease. *Nature* 2007;**447**(7143). Doi: 10.1038/nature05919.
7. Symonds ME., Budge H., Frazier-Wood AC. Epigenetics and Obesity: A Relationship Waiting to Be Explained. *Hum Hered* 2013;**75**(2–4):90–7. Doi: 10.1159/000352009.
8. Wegner M., Neddermann D., Piorunska-Stolzmann M., Jagodzinski PP. Role of epigenetic mechanisms in the development of chronic complications of diabetes. *Diabetes Res Clin Pract* 2014:164–75. Doi: 10.1016/j.diabres.2014.03.019.
9. Best WR., Becktel JM., Singleton JW., Kern F. Development of a Crohn's Disease Activity Index: National Cooperative Crohn's Disease Study. *Gastroenterology* 1976;**70**(3):439–44. Doi: 10.1016/S0016-5085(76)80163-1.
10. Van Assche G., Dignass A., Reinisch W., van der Woude CJ., Sturm A., De Vos M., et al. The second European evidence-based Consensus on the diagnosis and management of Crohn's disease: Special situations. *J Crohns Colitis* 2010;**4**(1):63–101. Doi: 10.1016/j.crohns.2009.09.009.
11. Dubois SG., Floyd EZ., Zvonic S., Kilroy G., Wu X., Carling S., et al. Isolation of human adipose-derived stem cells from biopsies and liposuction specimens. *Methods in Molecular Biology* 2008;**449**:69–79. Doi: 10.1007/978-1-60327-169-1_5.
12. Ceperuelo-Mallafré V., Ejarque M., Serena C., Duran X., Montori-Grau M., Rodríguez MA., et al. Adipose tissue glycogen accumulation is associated with obesity-linked inflammation in humans. *Mol Metab* 2016;**5**(1):5–18. Doi: 10.1016/j.molmet.2015.10.001.
13. Serena C., Keiran N., Ceperuelo-Mallafre V., Ejarque M., Fradera R., Roche K., et al. Obesity and Type 2 Diabetes Alters the Immune Properties of Human Adipose Derived Stem Cells. *Stem Cells* 2016;**34**(10):2559–73. Doi: 10.1002/stem.2429.
14. Serena C., Keiran N., Madeira A., Maymó-Masip E., Ejarque M., Terrón-Puig M., et al. Crohn's Disease Disturbs the Immune Properties of Human Adipose-Derived Stem Cells Related to Inflammasome Activation. *Stem Cell Reports* 2017;**9**(4):1109–23. Doi: 10.1016/j.stemcr.2017.07.014.
15. Titos E., Rius B., González-Périz A., López-Vicario C., Morán-Salvador E., Martínez-Clemente M., et al. Resolvin D1 and Its Precursor Docosahexaenoic Acid Promote Resolution of Adipose Tissue Inflammation by Eliciting Macrophage Polarization toward an M2-Like Phenotype. *The Journal of Immunology* 2011;**187**(10):5408–18. Doi: 10.4049/jimmunol.1100225.
16. Boronat-Toscano A., Vañó I., Monfort-Ferré D., Menacho M., Valldosera G., Caro A., et al. Smoking Suppresses the Therapeutic Potential of Adipose Stem Cells in Crohn's Disease Patients through Epigenetic Changes. *Cells* 2023;**12**(7):1021. Doi: 10.3390/cells12071021.
17. Pachón-Peña G., Serena C., Ejarque M., Petriz J., Duran X., Oliva-Olivera W., et al. Obesity Determines the Immunophenotypic Profile and Functional Characteristics of Human Mesenchymal Stem Cells From Adipose Tissue. *Stem Cells Transl Med* 2016;**5**(4):464–75. Doi: 10.5966/sctm.2015-0161.
18. Serena C., Keiran N., Madeira A., Maymó-Masip E., Ejarque M., Terrón-Puig M., et al. Crohn's Disease Disturbs the Immune Properties of Human Adipose-

Derived Stem Cells Related to Inflammasome Activation. *Stem Cell Reports* 2017;**9**(4):1109–23. Doi: 10.1016/j.stemcr.2017.07.014.
19. Moss J., Magenheim J., Neiman D., Zemmour H., Loyfer N., Korach A., et al. Comprehensive human cell-type methylation atlas reveals origins of circulating cell-free DNA in health and disease. *Nature Communications 2018 9:1* 2018;**9**(1):1–12. Doi: 10.1038/s41467-018-07466-6.
20. Loyfer N. GitHub - nloyfer/meth_atlas. Available at: https://github.com/nloyfer/meth_atlas?tab=License-1-ov-file#readme. Accessed March 5, 2024.
21. Assenov Y., Müller F., Lutsik P., Walter J., Lengauer T., Bock C. Comprehensive analysis of DNA methylation data with RnBeads. *Nat Methods* 2014;**11**(11). Doi: 10.1038/nmeth.3115.
22. Müller F., Scherer M., Assenov Y., Lutsik P., Walter J., Lengauer T., et al. RnBeads 2.0: Comprehensive analysis of DNA methylation data. *Genome Biol* 2019;**20**(1). Doi: 10.1186/s13059-019-1664-9.
23. Smith ML., Baggerly KA., Bengtsson H., Ritchie ME., Hansen KD. illuminaio: An open source IDAT parsing tool for Illumina microarrays. *F1000Res* 2013;**2**. Doi: 10.12688/f1000research.2-264.v1.
24. Johnson WE., Li C., Rabinovic A. Adjusting batch effects in microarray expression data using empirical Bayes methods. *Biostatistics* 2007;**8**(1). Doi: 10.1093/biostatistics/kxj037.
25. Leek JT., Johnson WE., Parker HS., Jaffe AE., Storey JD. The SVA package for removing batch effects and other unwanted variation in high-throughput experiments. *Bioinformatics* 2012;**28**(6). Doi: 10.1093/bioinformatics/bts034.
26. Leek JT JWPHFEJAZYSJTL. Bioconductor - sva. Bioconductor. Doi: 10.18129/B9.bioc.sva.
27. Teschendorff AE., Marabita F., Lechner M., Bartlett T., Tegner J., Gomez-Cabrero D., et al. A beta-mixture quantile normalization method for correcting probe design bias in Illumina Infinium 450 k DNA methylation data. *Bioinformatics* 2013;**29**(2). Doi: 10.1093/bioinformatics/bts680.
28. Aryee MJ., Jaffe AE., Corrada-Bravo H., Ladd-Acosta C., Feinberg AP., Hansen KD., et al. Minfi: A flexible and comprehensive Bioconductor package for the analysis of Infinium DNA methylation microarrays. *Bioinformatics* 2014;**30**(10). Doi: 10.1093/bioinformatics/btu049.
29. Jaffe AE., Murakami P., Lee H., Leek JT., Fallin MD., Feinberg AP., et al. Bump hunting to identify differentially methylated regions in epigenetic epidemiology studies. *Int J Epidemiol* 2012;**41**(1). Doi: 10.1093/ije/dyr238.
30. Wilhelm-Benartzi CS., Koestler DC., Karagas MR., Flanagan JM., Christensen BC., Kelsey KT., et al. Review of processing and analysis methods for DNA methylation array data. *Br J Cancer* 2013:1394–402. Doi: 10.1038/bjc.2013.496.
31. Bibikova M., Barnes B., Tsan C., Ho V., Klotzle B., Le JM., et al. High density DNA methylation array with single CpG site resolution. *Genomics* 2011;**98**(4):288–95. Doi: 10.1016/j.ygeno.2011.07.007.
32. Hoffman GE., Schadt EE. variancePartition: Interpreting drivers of variation in complex gene expression studies. *BMC Bioinformatics* 2016;**17**(1). Doi: 10.1186/s12859-016-1323-z.
33. Ewels P., Magnusson M., Lundin S., Käller M. MultiQC: Summarize analysis results for multiple tools and samples in a single report. *Bioinformatics* 2016;**32**(19). Doi: 10.1093/bioinformatics/btw354.

34. Bolger AM., Lohse M., Usadel B. Trimmomatic: A flexible trimmer for Illumina sequence data. *Bioinformatics* 2014;**30**(15). Doi: 10.1093/bioinformatics/btu170.
35. Dobin A., Davis CA., Schlesinger F., Drenkow J., Zaleski C., Jha S., et al. STAR: Ultrafast universal RNA-seq aligner. *Bioinformatics* 2013;**29**(1). Doi: 10.1093/bioinformatics/bts635.
36. Love MI., Huber W., Anders S. Moderated estimation of fold change and dispersion for RNA-seq data with DESeq2. *Genome Biol* 2014;**15**(12). Doi: 10.1186/s13059-014-0550-8.
37. Zhu A., Ibrahim JG., Love MI. Heavy-Tailed prior distributions for sequence count data: Removing the noise and preserving large differences. *Bioinformatics* 2019;**35**(12). Doi: 10.1093/bioinformatics/bty895.
38. Blighe K., Rana S., Lewis M. *Publication-ready volcano plots with enhanced colouring and labeling*. 2022.
39. Subramanian A., Tamayo P., Mootha VK., Mukherjee S., Ebert BL., Gillette MA., et al. Gene set enrichment analysis: a knowledge-based approach for interpreting genome-wide expression profiles. *Proc Natl Acad Sci U S A* 2005;**102**(43):15545–50. Doi: 10.1073/PNAS.0506580102.
40. Liberzon A., Subramanian A., Pinchback R., Thorvaldsdóttir H., Tamayo P., Mesirov JP. Molecular signatures database (MSigDB) 3.0. *Bioinformatics* 2011;**27**(12):1739–40. Doi: 10.1093/BIOINFORMATICS/BTR260.
41. Korotkevich G., Sukhov V., Budin N., Shpak B., Artyomov MN., Sergushichev A. Fast gene set enrichment analysis n.d. Doi: 10.1101/060012.
42. Wickham H. *ggplot2: Elegant Graphics for Data Analysis. Springer-Verlag New York*. vol. 35. 2016.
43. Jaffe AE., Murakami P., Lee H., Leek JT., Fallin MD., Feinberg AP., et al. Bump hunting to identify differentially methylated regions in epigenetic epidemiology studies. *Int J Epidemiol* 2012;**41**(1):200–9. Doi: 10.1093/IJE/DYR238.
44. Lu XC., Tang L., Li K., Zheng J., Zhao P., Tao Y., et al. Contribution of NKX2-3 Polymorphisms to Inflammatory Bowel Diseases: A Meta-Analysis of 35358 subjects. *Scientific Reports 2014 4:1* 2014;**4**(1):1–9. Doi: 10.1038/srep03924.
45. Lessard JC., Piña-Paz S., Rotty JD., Hickerson RP., Kaspar RL., Balmain A., et al. Keratin 16 regulates innate immunity in response to epidermal barrier breach. *Proc Natl Acad Sci U S A* 2013;**110**(48):19537–42. Doi: 10.1073/PNAS.1309576110/SUPPL_FILE/PNAS.201309576SI.PDF.
46. Grünberg JR., Elvin J., Paul A., Hedjazifar S., Hammarstedt A., Smith U. CCN5/WISP2 and metabolic diseases. *J Cell Commun Signal* 2018;**12**(1):309–18. Doi: 10.1007/S12079-017-0437-Z.
47. Segawa Y., Muneta T., Makino H., Nimura A., Mochizuki T., Ju YJ., et al. Mesenchymal stem cells derived from synovium, meniscus, anterior cruciate ligament, and articular chondrocytes share similar gene expression profiles. *J Orthop Res* 2009;**27**(4):435–41. Doi: 10.1002/JOR.20786.
48. Yu W., Hegarty JP., Berg A., Chen X., West G., Kelly AA., et al. NKX2-3 transcriptional regulation of endothelin-1 and VEGF signaling in human intestinal microvascular endothelial cells. *PLoS One* 2011;**6**(5). Doi: 10.1371/JOURNAL.PONE.0020454.
49. Serena C., Queipo-Ortuño M., Millan M., Sanchez-Alcoholado L., Caro A., Espina B., et al. Microbial Signature in Adipose Tissue of Crohn's Disease Patients. *J Clin Med* 2020;**9**(8):2448. Doi: 10.3390/jcm9082448.
50. Ha CWY., Martin A., Sepich-Poore GD., Shi B., Wang Y., Gouin K., et al. Translocation of Viable Gut Microbiota to Mesenteric Adipose Drives Formation

of Creeping Fat in Humans. *Cell* 2020;**183**(3):666-683.e17. Doi: 10.1016/j.cell.2020.09.009.
51. Monfort-Ferré D., Caro A., Menacho M., Martí M., Espina B., Boronat-Toscano A., et al. The Gut Microbiota Metabolite Succinate Promotes Adipose Tissue Browning in Crohn's Disease. *J Crohns Colitis* 2022;**16**(10):1571–83. Doi: 10.1093/ECCO-JCC/JJAC069.
52. Ihara S., Hirata Y., Koike K. TGF-β in inflammatory bowel disease: a key regulator of immune cells, epithelium, and the intestinal microbiota. *J Gastroenterol* 2017;**52**(7):777–87. Doi: 10.1007/S00535-017-1350-1.
53. Mariani M., Baldessari D., Francisconi S., Viggiano L., Rocchi M., Zappavigna V., et al. Two murine and human homologs of mab-21, a cell fate determination gene involved in Caenorhabditis elegans neural development. *Hum Mol Genet* 1999;**8**(13):2397–406. Doi: 10.1093/HMG/8.13.2397.
54. Xie L., Huang R., Huang H., Liu X., Yu J. Transcriptomics and Metabolomics Identify Drug Resistance of Dormant Cell in Colorectal Cancer. *Front Pharmacol* 2022;**13**. Doi: 10.3389/fphar.2022.879751.
55. Serena C., Millan M., Ejarque M., Saera-Vila A., Maymó-Masip E., Núñez-Roa C., et al. Adipose stem cells from patients with Crohn's disease show a distinctive DNA methylation pattern. *Clin Epigenetics* 2020;**12**(1). Doi: 10.1186/s13148-020-00843-3.
56. Li E., Beard C., Jaenisch R. Role for DNA methylation in genomic imprinting. *Nature* 1993;**366**(6453). Doi: 10.1038/366362a0.
57. Li Z., Lei H., Luo M., Wang Y., Dong L., Ma Y., et al. DNA methylation downregulated mir-10b acts as a tumor suppressor in gastric cancer. *Gastric Cancer* 2015;**18**(1). Doi: 10.1007/s10120-014-0340-8.
58. Markov AV., Babushkina NP., Golubenko MV., Salakhov RR., Sharysh DV., Zarubin AA., et al. DNA methylation within genes of microRNA MIR-10B and transcription factor TWIST1 in atherosclerosis. *Atherosclerosis* 2020;**315**. Doi: 10.1016/j.atherosclerosis.2020.10.289.
59. Abdelmaksoud-Dammak R., Chamtouri N., Triki M., Saadallah-Kallel A., Ayadi W., Charfi S., et al. Overexpression of miR-10b in colorectal cancer patients: Correlation with TWIST-1 and E-cadherin expression. *Tumor Biology* 2017;**39**(3). Doi: 10.1177/1010428317695916.
60. Nazarenko MS., Markov A V., Lebedev IN., Freidin MB., Sleptcov AA., Koroleva IA., et al. A comparison of genome-wide DNA methylation patterns between different vascular tissues from patients with coronary heart disease. *PLoS One* 2015;**10**(4). Doi: 10.1371/journal.pone.0122601.
61. Shi Y., Sun X., He X. Overexpression of aristaless-like homeobox-4 inhibits proliferation, invasion, and EMT in hepatocellular carcinoma cells. *Oncol Res* 2017;**25**(1). Doi: 10.3727/096504016X14685034103833.
62. Zogg H., Singh R., Ha SE., Wang Z., Jin B., Ha M., et al. miR-10b-5p rescues leaky gut linked with gastrointestinal dysmotility and diabetes. *United European Gastroenterol J* 2023;**11**(8). Doi: 10.1002/ueg2.12463.
63. Lu Y., Yang L., Qin A., Qiao Z., Huang B., Jiang X., et al. miR-1470 regulates cell proliferation and apoptosis by targeting ALX4 in hepatocellular carcinoma. *Biochem Biophys Res Commun* 2020;**522**(3). Doi: 10.1016/j.bbrc.2019.10.139.
64. Zhao J., Chen H qiang., Yang H fang., Li Y., Chen D jiao., Huang Y jing., et al. Epigenetic silencing of ALX4 regulates microcystin-LR induced hepatocellular carcinoma through the P53 pathway. *Science of the Total Environment* 2019;**683**. Doi: 10.1016/j.scitotenv.2019.05.144.

65. Li Yim AYF., Duijvis NW., Zhao J., de Jonge WJ., D'Haens GRAM., Mannens MMAM., et al. Peripheral blood methylation profiling of female Crohn's disease patients. *Clin Epigenetics* 2016;**8**(1). Doi: 10.1186/s13148-016-0230-5.
66. Joustra V., Li Yim AYF., Hageman I., Levin E., Adams A., Satsangi J., et al. Long-term Temporal Stability of Peripheral Blood DNA Methylation Profiles in Patients With Inflammatory Bowel Disease. *CMGH* 2023;**15**(4). Doi: 10.1016/j.jcmgh.2022.12.011.
67. Joustra V., Hageman IL., Satsangi J., Adams A., Ventham NT., De Jonge WJ., et al. Systematic Review and Meta-analysis of Peripheral Blood DNA Methylation Studies in Inflammatory Bowel Disease. *J Crohns Colitis* 2023;**17**(2). Doi: 10.1093/ecco-jcc/jjac119.
68. Ventham NT., Kennedy NA., Adams AT., Kalla R., Heath S., O'Leary KR., et al. Integrative epigenome-wide analysis demonstrates that DNA methylation may mediate genetic risk in inflammatory bowel disease. *Nat Commun* 2016;**7**. Doi: 10.1038/ncomms13507.
69. Yu W., Lin Z., Kelly AA., Hegarty JP., Poritz LS., Wang Y., et al. Association of a Nkx2-3 polymorphism with Crohn's disease and expression of Nkx2-3 is up-regulated in B cell lines and intestinal tissues with Crohn's disease. *J Crohns Colitis* 2009;**3**(3):189–95. Doi: 10.1016/J.CROHNS.2009.04.003.
70. Qian W., Xu Y., Wen W., Huang L., Guo Z., Zhu W., et al. Exosomal miR-103a-3p from Crohn's Creeping Fat-Derived Adipose-Derived Stem Cells Contributes to Intestinal Fibrosis by Targeting TGFBR3 and Activating Fibroblasts. *J Crohns Colitis* 2023;**17**(8). Doi: 10.1093/ecco-jcc/jjad042.
71. Marger F., Gelot A., Alloui A., Matricon J., Sanguesa Ferrer JF., Barrère C., et al. T-type calcium channels contribute to colonic hypersensitivity in a rat model of irritable bowel syndrome. *Proc Natl Acad Sci U S A* 2011;**108**(27):11268–73. Doi: 10.1073/PNAS.1100869108.
72. Scanzi J., Accarie A., Muller E., Pereira B., Aissouni Y., Goutte M., et al. Colonic overexpression of the T-type calcium channel Ca v 3.2 in a mouse model of visceral hypersensitivity and in irritable bowel syndrome patients. *Neurogastroenterol Motil* 2016;**28**(11):1632–40. Doi: 10.1111/NMO.12860.
73. Picard E., Carvalho FA., Agosti F., Bourinet E., Ardid D., Eschalier A., et al. Inhibition of Cav3.2 calcium channels: A new target for colonic hypersensitivity associated with low-grade inflammation. *Br J Pharmacol* 2019;**176**(7):950–63. Doi: 10.1111/BPH.14608.
74. Halpin SJ., Ford AC. Prevalence of symptoms meeting criteria for irritable bowel syndrome in inflammatory bowel disease: Systematic review and meta-analysis. *American Journal of Gastroenterology* 2012:1474–82. Doi: 10.1038/ajg.2012.260.

FIGURE LEGENDS

Figure 1. **Exploratory data analysis. (A)** Summary of study design with the main differences found among groups. **(B)** Plot of the two principal components of the overall DNA-methylation and RNAseq profiles in ASCs isolated from non-CD (in grey), active CD (in blue) and inactive CD (in orange) groups, and in different location of adipose tissue: hMAT (triangle) and CF

(circle) for ASCs isolated from patients with active CD. **(C)** Heatmaps of the top 50 most significant DMPs and DEGs among the groups. Red bars represent the hypermethylated positions and higher expression and blue bars represent the hypomethylated positions and lower expression. Abbreviations: CD, Crohn's disease; ASCs, adipose-stem cells; CF, creeping fat; hMAT, healthy mesenteric adipose tissue; DMP; differentially methylated position; DMR, differentially methylated region; DEG, differentially expressed genes; PC, principal component.

Figure 2. Analysis of DMPs reveals only small changes in ASC isolated from CD with different clinical activity. (A) Distribution of DMPs significant probes and all EPIC probes. Approximately 5% of all significant probes of the DMPs are located in the island and 17% of EPIC probes of the DMPs are located in the island. **(B)** Volcano plot showing differentially methylated promoters in ASCs from CD subject compared to non-CD subjects. Significant hits with adjusted p-value <0.05 are in red. The right of the X axis indicates the hypomethylation in ASCs from CD, and the left of the X axis indicates hypermethylation CD-ASCs. Gene symbols shown correspond to known genes associated with significant differentially methylated promoter regions; asterisks indicate no known gene in the promoter region annotation **(C)** DMR plot in MAB21L2 gene. **(D)** Contribution to the beta variance by different variables (Crohn's disease, hospital, gender, smoking, CRP) using the VariancePartition R package.
Abbreviations: CD, Crohn's disease; DMP, differentially methylated position; ASCs, adipose-stem cells; DMP, differentially methylated position; CRP, high sensitive C-reactive protein; aCD, active Crohn's disease; iCD, inactive Crohn's disease; hMAT, healthy mesenteric adipose tissue.

Figure 3: Transcriptomic profiling of ASCs reveals that CD is associated with an up-regulation of immune response and stress-related genes. (A) Venn diagram of the relationship among differentially expressed genes (DEGs) in ASCs from non-CD, active CD and inactive CD groups. **(B)** In the left panel, a volcano plot shows differential gene expression between ASCs isolated from non-CD (hMAT n=7) and active CD (CF n=7; hMAT n=7). Significant genes with adjusted p-value <0.05 are in red. The right of the X axis indicates the gene expression elevated in ASCs from active CD, and the left of the X axis indicates the gene expression elevated in non-CD-ASCs. The normalised enrichment score (NES from GSEA) is shown in the right panel. Red circles highlight the pathways up-regulated in active CD and blue circles highlight pathways down-regulated in active CD. **(C)** Volcano plot showing differentially gene expression between ASCs isolated from non-CD (hMAT n=7) and inactive CD (hMAT n=7). The normalised enrichment score (NES from GSEA) is shown in the right panel. Red circles indicate the pathways up-regulated in inactive CD and blue circles indicate the down-regulated pathways in inactive CD. **(D)** Volcano plot showing differential gene expression between ASCs isolated from active CD (CF n=7; hMAT n=7) and inactive CD (hMAT n=7) groups.

Abbreviations: CD, Crohn's disease; aCD, active Crohn's disease; iCD, inactive Crohn's disease; ASCs, adipose-stem cells; DMP; differentially methylated position; DEG, differentially expressed genes.

Figure 4: Integration of DNA methylation and gene expression identifies elevated *MAB21L2* expression in adipose tissue of CD. (A) DNA methylation, gene expression and correlation of *MAB21L2* in ASCs isolated from non-CD (n=7; in grey) and active (n=6 from CF, n=7 from hMAT; in blue) CD groups. **(B)** DNA methylation, gene expression and correlation of *MAB21L2* in ASCs isolated from non-CD (n=7; in grey) and inactive CD (n=5; in orange). **(C)** *MAB21L2* gene expression performed by qPCR in ASCs from non-CD and from inactive and active CD (n=7 per group). *p<0.05 vs non-CD-ASCs. **(D)** *MAB21L2* expression by qPCR in visceral adipose tissue and subcutaneous adipose tissue among non-CD (n=5), inactive (n=5) and active (n=7) CD. *p<0.05 vs non-CD MAT, $^{\$}p$<0.01 as indicated in the figure **(E)** *MAB21L2* gene expression of adipose tissue constituents of active CD: mature adipocyte (n=7), ATMs (n=6) and ASCs (n=7). *p<0.05, ***p<0.0001 vs mature adipocytes **(F)** *MAB21L2* gene expression of PBMCs in non-CD (n=3), inactive CD (n=6) and active CD (n=4). **(G)** Positive correlation between *MAB21L2* gene expression in ASCs and hsCRP in serum (mg/dl). Bars in graphs represent mean ±SEM.

Abbreviations: CD, Crohn's disease; ASCs, adipose-stem cells; ATMs, adipose tissue macrophages; SAT, subcutaneous adipose tissue; MAT, mesenteric adipose tissue; PBMCs, peripheral blood mononuclear cells; hsCRP, high-sensitivity C-reactive protein.

Figure 5: *CACNA1H* gene might be an important player in CD during remission. (A) DNA methylation, gene expression and correlation of *CACNA1H* in ASCs isolated from non-CD (n= 7; in grey) and inactive CD (n=5; in orange). **(B)** DNA methylation, gene expression and correlation of *CACNA1H* in ASCs isolated from active CD (n=6; in blue) and inactive CD (n=5; in orange). **(C)** *CACNA1H* gene expression performed by qPCR with ASCs isolated from non-CD (n=5), inactive CD (n=5) and active CD (n=7). $^{\$}p$<0.05 as indicated in the figure **(D)** *CACNA1H* expression in visceral adipose tissue and subcutaneous adipose tissue among non-CD (n=4), inactive CD (n=4) and active CD (n=6). *p<0.05 vs non-CD MAT, $^{\$}p$<0.05 as indicated in the figure, **(E)** *CACNA1H* expression of adipose tissue constituents of inactive CD: visceral adipose tissue (n=5), mature adipocytes (n=5), and ASCs (n=5). *p<0.05, ****p<0.0001 vs MAT, $^{\$\$}p$<0.005 as indicated in the figure **(F)** *CACNA1H* expression in PBMCs among non-CD (n=3), inactive CD (n=6) and active CD (n=4). $^{\$}p$<0.05 as indicated in the figure **(G)** Negative correlation between *CACNA1H* expression in ASCs and hsCRP in serum (mg/dl). Bars in graphs represent mean ±SEM.

Abbreviations: CD, Crohn's disease; ASCs, adipose-stem cells; SAT, subcutaneous adipose tissue; MAT, mesenteric adipose tissue; PBMCs, peripheral blood mononuclear cells, hsCRP, high-sensitivity C-reactive protein.

Table 1. Demographic characteristics and clinical data.

	Non-CD	Active CD		Inactive CD
	(SAT/ hMAT-VAT)	(SAT/ CF-VAT)	(hMAT-VAT)	(SAT/ hMAT-VAT)
N	7	7	7	7
Sex (male/female)	4/3	3/4	4/3	1/6
Age (years)	49.86 ± 7.38	42,71 ± 13.26	44 ± 13.42	54.14 ± 14.35
BMI (kg/m^2)	22.30 ± 2.29	24.46 ± 2.91	23.43 ± 3.84	25.19 ± 4.62
C-reactive protein (mg/dL)	0.4	3.08 ± 3.98[a,b]	3.71 ± 3.87 [a,b]	0.43 ± 0.21
Smoking status, n (%)				
Current smoker	2 (28.6)	5 (71)	3 (42.8)	1 (14)
Ex-smoker	0	1 (14)	2 (28.6)	5 (71)
Never smoker	5 (71.4)	1 (14)	2 (28.6)	1 (14)
Age at diagnosis, n (%)				
A1	-	0	0	1 (14)
A2	-	5 (71)	4 (57)	2 (29)
A3	-	2 (29)	3 (43)	4 (57)
Location, n (%)				
L1	-	6 (86)	7 (100)	5 (71)
L2	-	0	0	1 (14)
L3	-	1 (14)	0	1 (14)
Behaviour, n (%)				
B1	-	0	0	5 (71)
B2	-	4 (57)	2 (29)	1 (14)
B3	-	3 (43)	5 (71)	1 (14)
Immunosuppresors (Thiopurines), n (%)	-	3 (50)	2 (29)	4 (57)
Anti-TNF treatment, n (%)	-	0	3(43)	0
Last attack (months)	-	-	-	22 ± 28.51

Abbreviations: CD, Crohn Disease; SAT, subcutaneous adipose tissue; VAT, visceral adipose tissue; CF, creeping fat; hMAT, healthy mesenteric adipose tissue; BMI, body mass index. Age at diagnosis: A1>16 years; A2 17–40 years; A3 > 40 years; Location: L1 = ileal; L2 = colonic; L3 = ileocolonic; Behaviour: B1 = non-stenotic, non-fistulising Crohn's disease; B2 = stenotic Crohn's disease; B3 = fistulising Crohn's disease. Results are presented as mean ± SD. ANOVA followed by post hoc Bonferroni test was used to compare means between groups.

[a] $p < 0.01$ significant differences compared with non-CD

[b] $p < 0.05$ significant differences compared with inactive disease.

Table 2. Summary of cell types isolated, and tissues used in the study.

Adipose tissue biopsies	**Active CD**			**Inactive CD**		**Non-CD**		**Employed in:**
	VAT		SAT	VAT	SAT	VAT	SAT	
	CF	hMAT		hMAT		hMAT		
ASCs isolation	√	√		√		√		DNA Methylation, Transcriptomics, integration studies
ATMs isolation	√							Validation of candidate's genes by qPCR obtained from the integrative analysis (DMPs and DEGs) in different cell subtypes and tissues
Mature Adipocytes	√			√				
Total tissue	√	√	√	√	√	√	√	

Abbreviations: VAT, visceral adipose tissue; SAT, subcutaneous adipose tissue; CF, creeping fat; hMAT, healthy mesenteric adipose tissue, ASCs, adipose-derived stem cells, ATMs, adipose tissue macrophages.

Figure 1

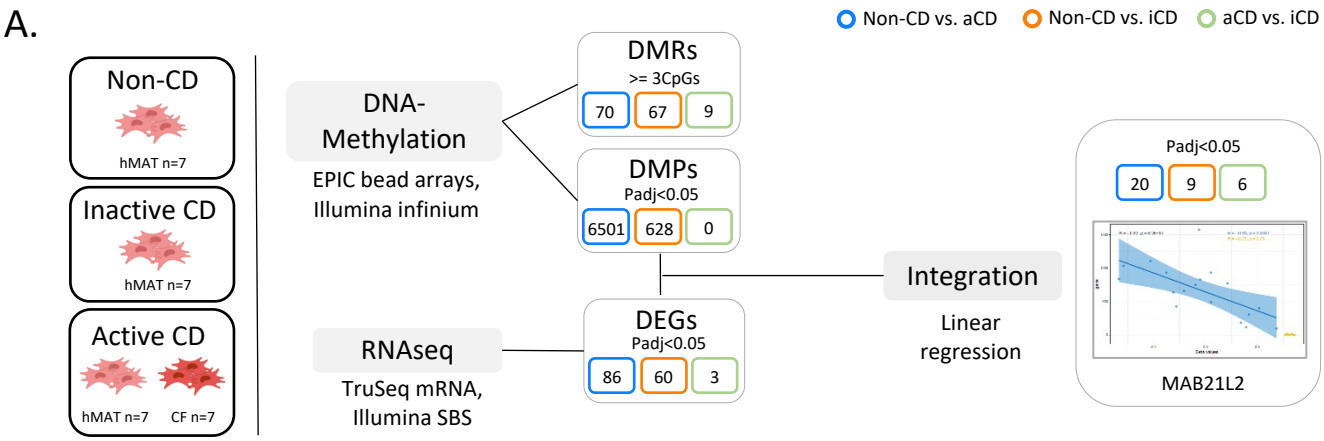
A.
Non-CD vs. aCD
Non-CD vs. iCD
aCD vs. iCD
Non-CD
hMAT n=7
Inactive CD
hMAT n=7
Active CD
hMAT n=7
CF n=7
DNA-Methylation
EPIC bead arrays, Illumina infinium
DMRs
>= 3CpGs
70
67
9
DMPs
Padj<0.05
6501
628
0
RNAseq
TruSeq mRNA, Illumina SBS
DEGs
Padj<0.05
86
60
3
Integration
Linear regression
Padj<0.05
20
9
6
MAB21L2

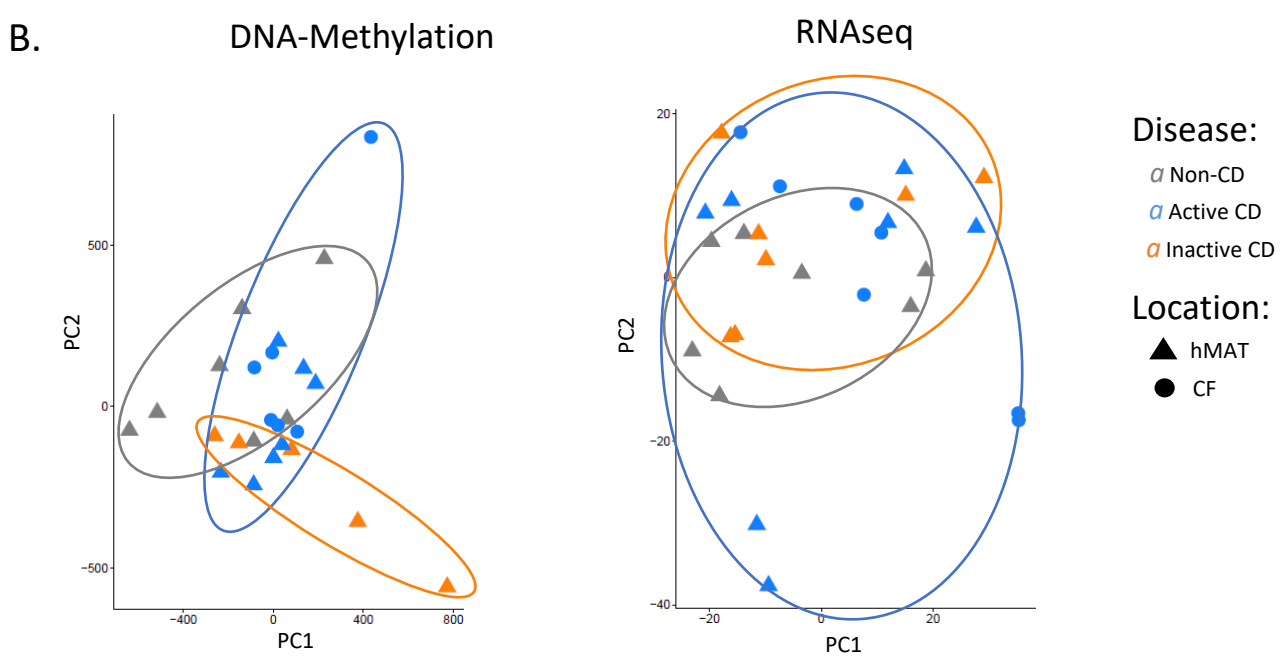
B.
DNA-Methylation
RNAseq
PC1
PC2
Disease:
Non-CD
Active CD
Inactive CD
Location:
hMAT
CF

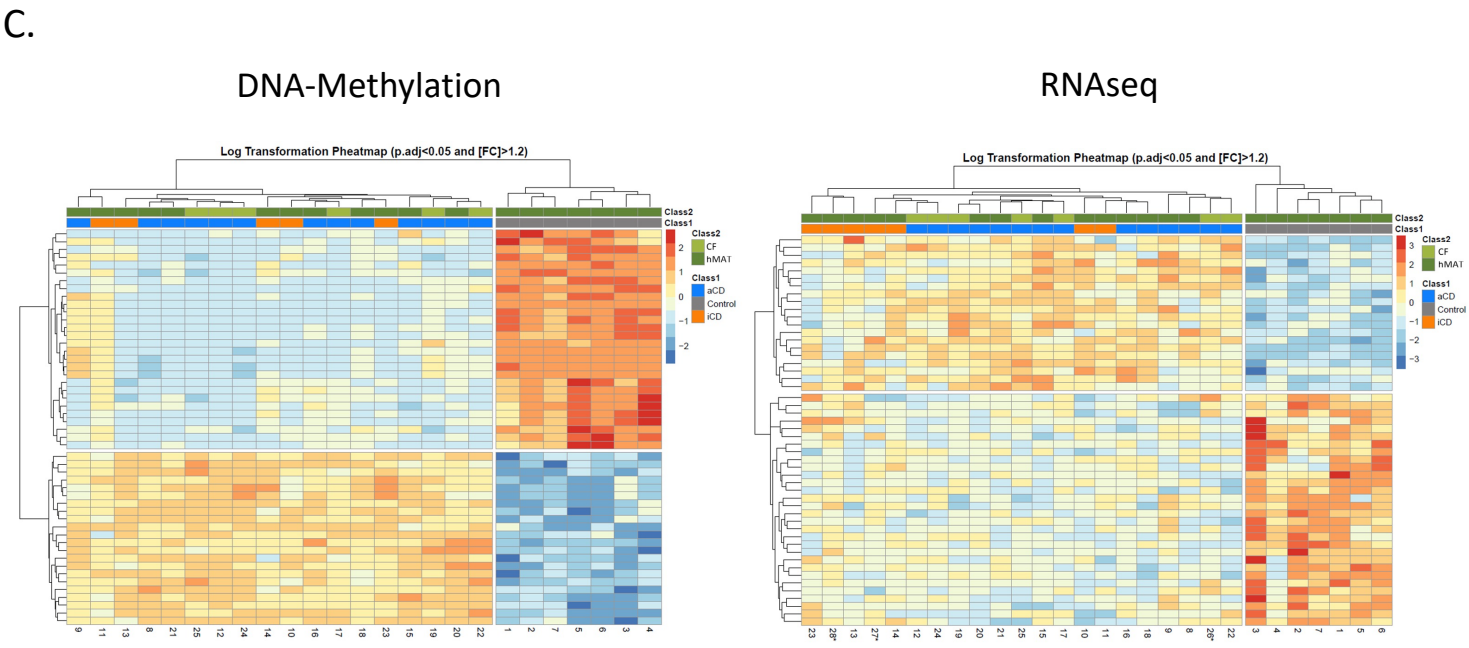
C.
DNA-Methylation
RNAseq
Log Transformation Pheatmap (p.adj<0.05 and [FC]>1.2)
Log Transformation Pheatmap (p.adj<0.05 and [FC]>1.2)
Class2
Class1
CF
hMAT
aCD
Control
iCD

Figure 2

A.

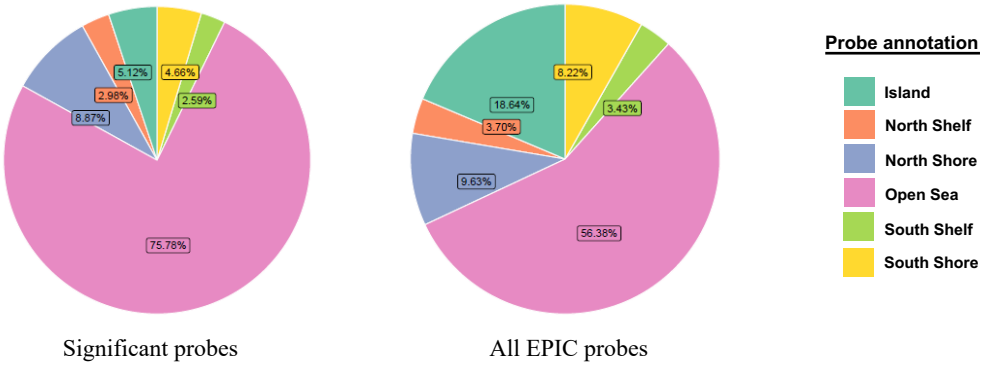

Significant probes All EPIC probes

B.

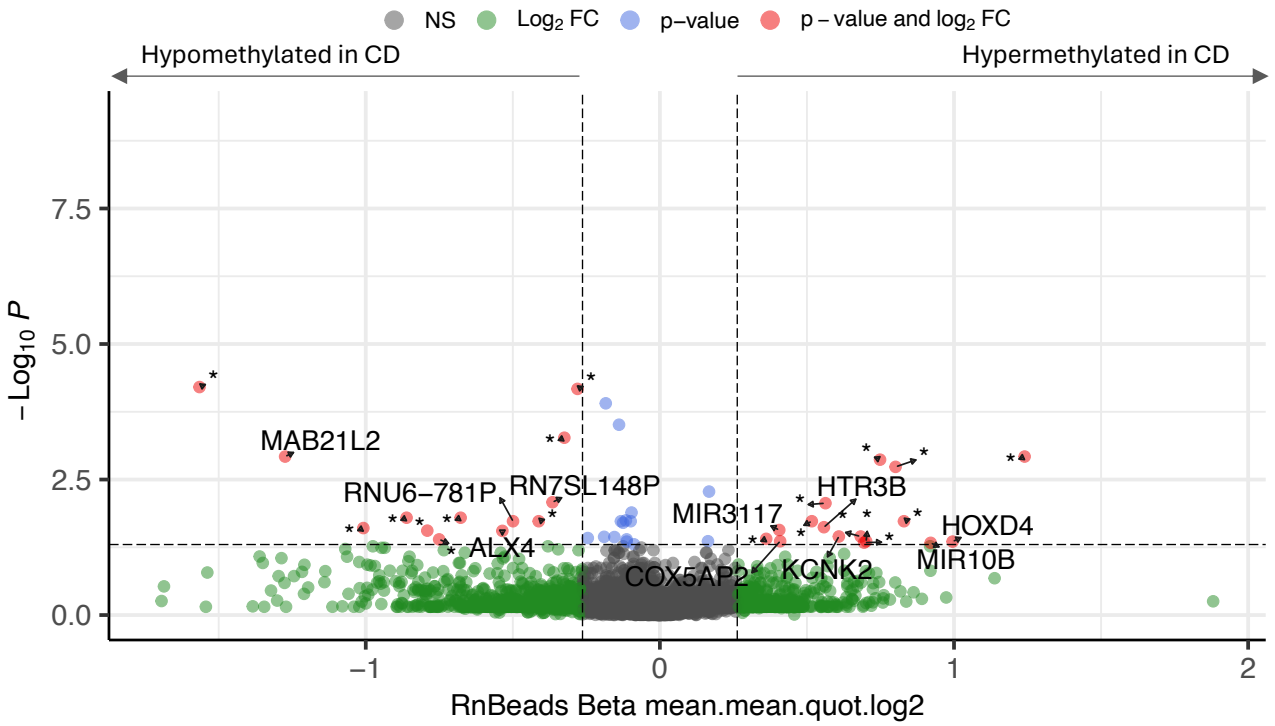

C.

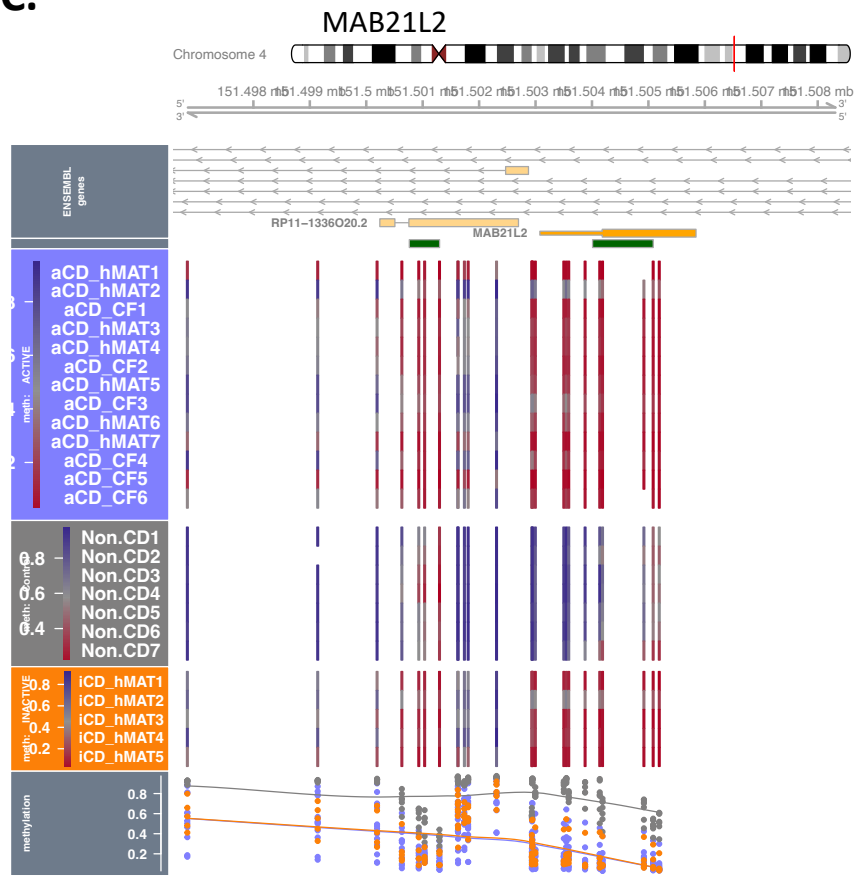

D.

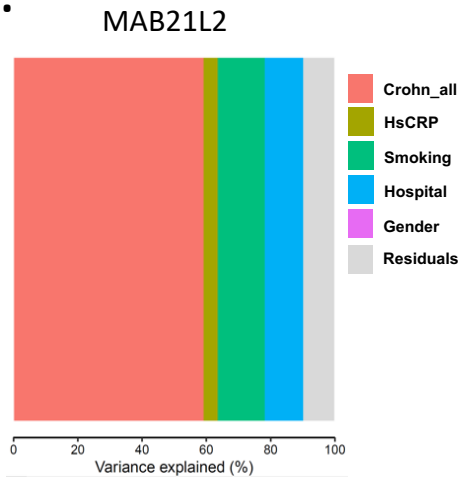

Figure 3

A.

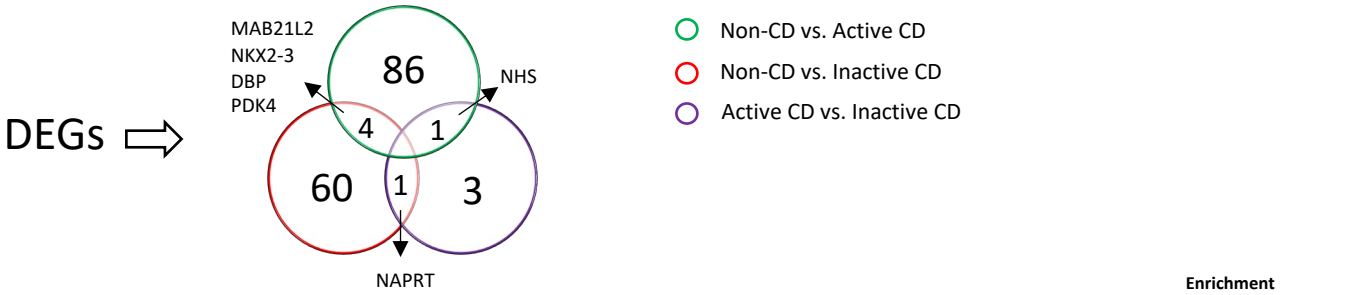

B.

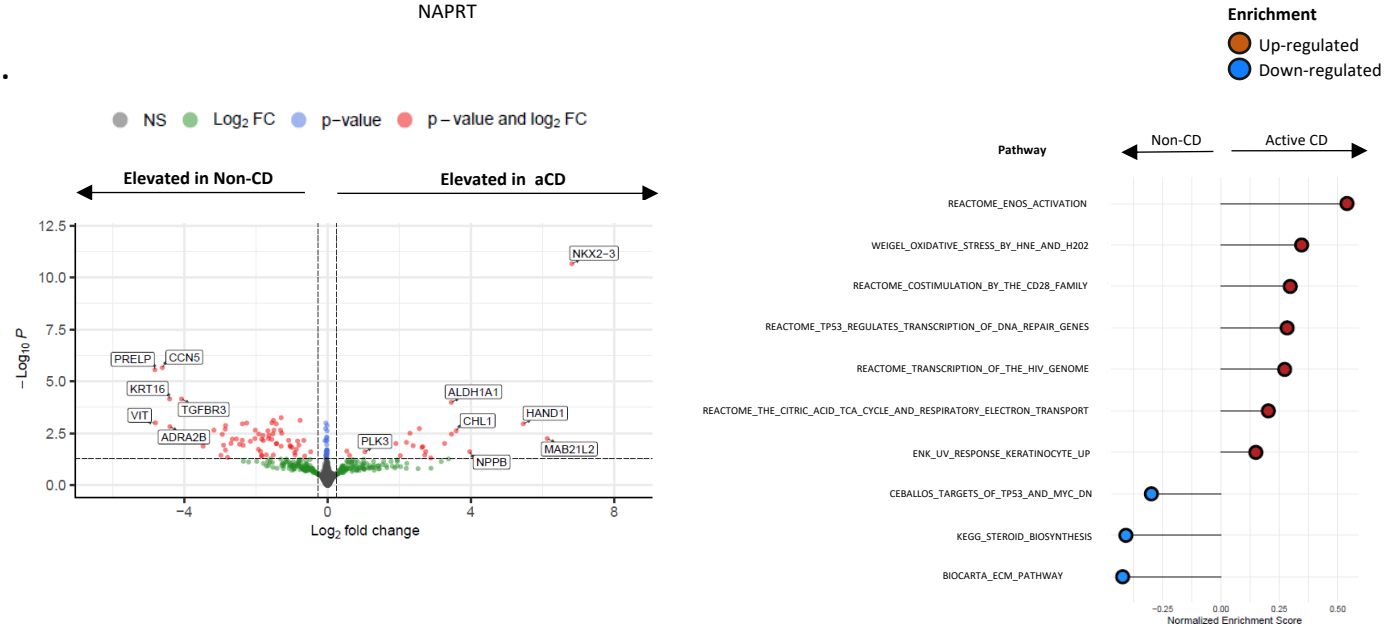

C.

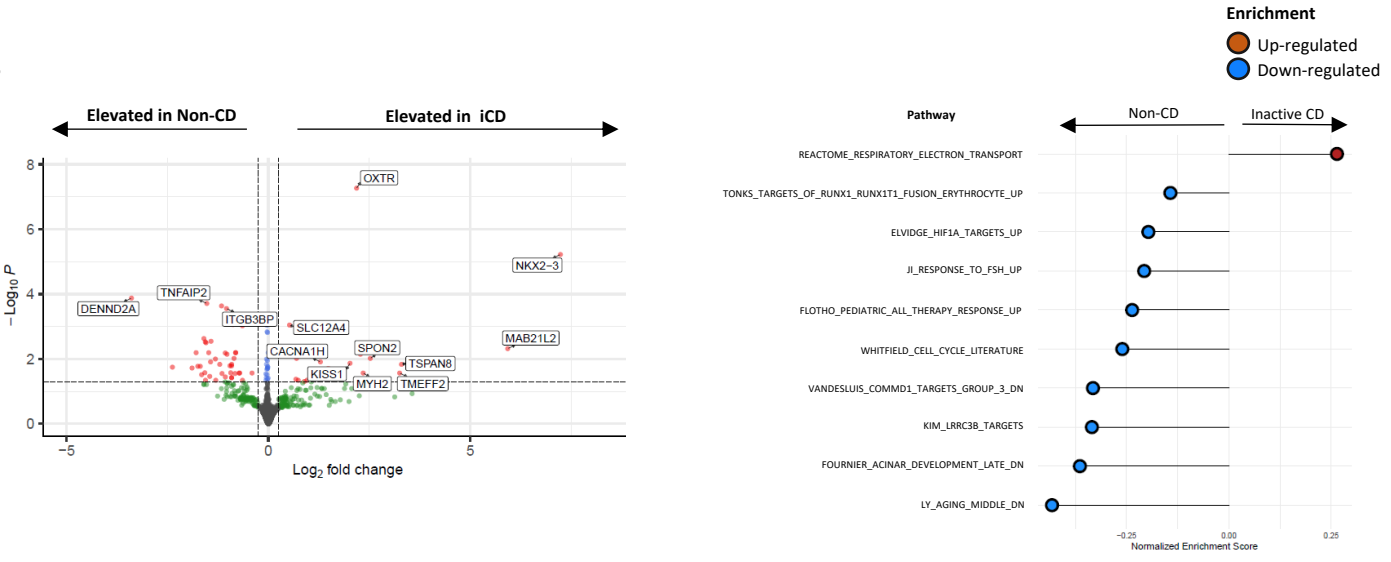

D.

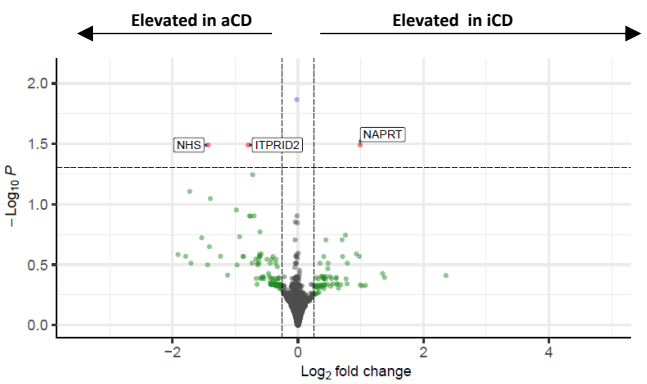

Figure 4

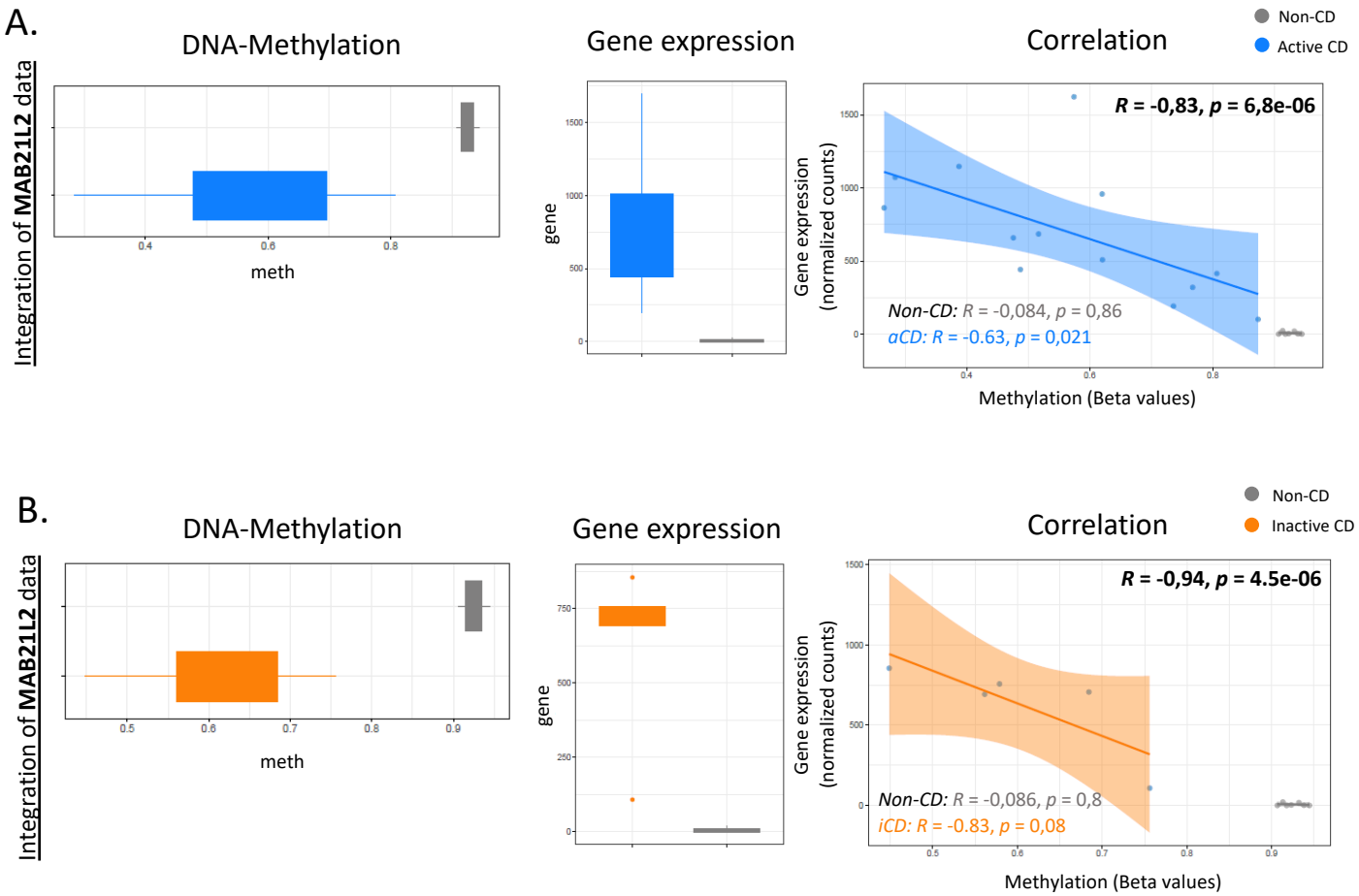
A.
DNA-Methylation
Gene expression
Correlation
Non-CD
Active CD
Integration of MAB21L2 data
meth
gene
Gene expression (normalized counts)
R = -0,83, p = 6,8e-06
Non-CD: R = -0,084, p = 0,86
aCD: R = -0.63, p = 0,021
Methylation (Beta values)
B.
DNA-Methylation
Gene expression
Correlation
Non-CD
Inactive CD
Integration of MAB21L2 data
meth
gene
Gene expression (normalized counts)
R = -0,94, p = 4.5e-06
Non-CD: R = -0,086, p = 0,8
iCD: R = -0.83, p = 0,08
Methylation (Beta values)

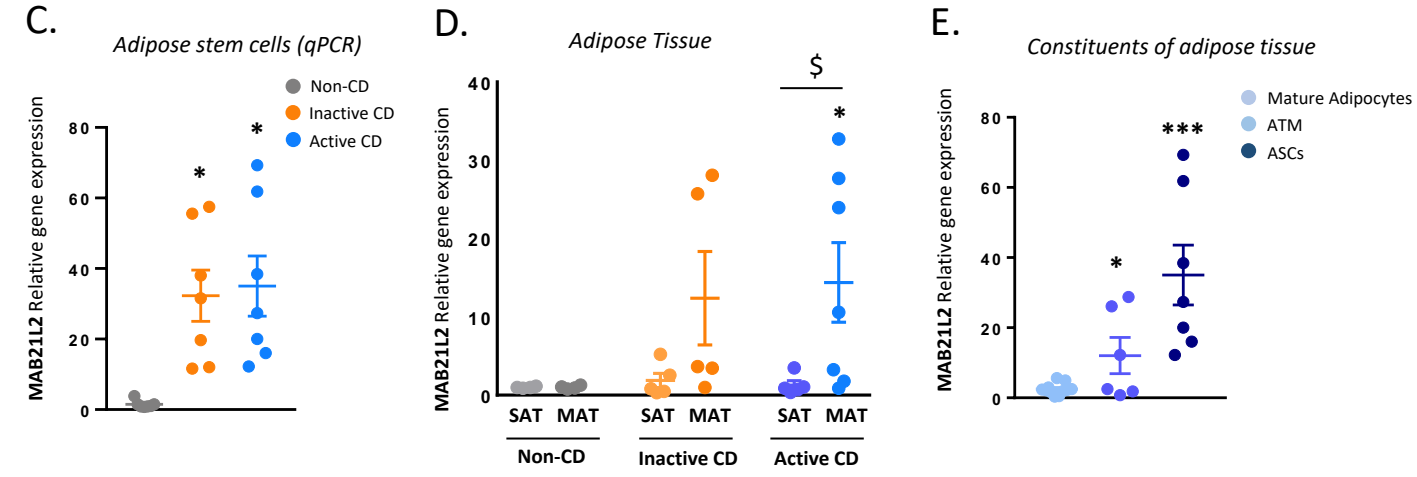
C.
Adipose stem cells (qPCR)
Non-CD
Inactive CD
Active CD
MAB21L2 Relative gene expression
D.
Adipose Tissue
$
MAB21L2 Relative gene expression
SAT MAT
Non-CD
Inactive CD
Active CD
E.
Constituents of adipose tissue
Mature Adipocytes
ATM
ASCs
MAB21L2 Relative gene expression

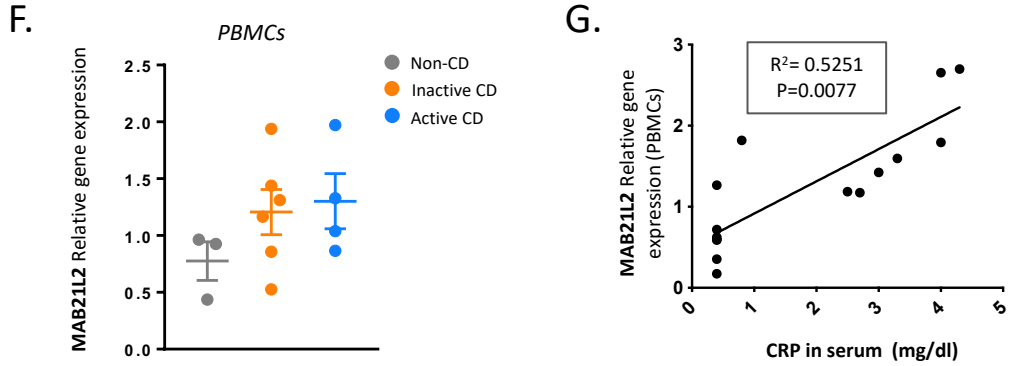
F.
PBMCs
Non-CD
Inactive CD
Active CD
MAB21L2 Relative gene expression
G.
R²= 0.5251
P=0.0077
MAB21L2 Relative gene expression (PBMCs)
CRP in serum (mg/dl)

Figure 5

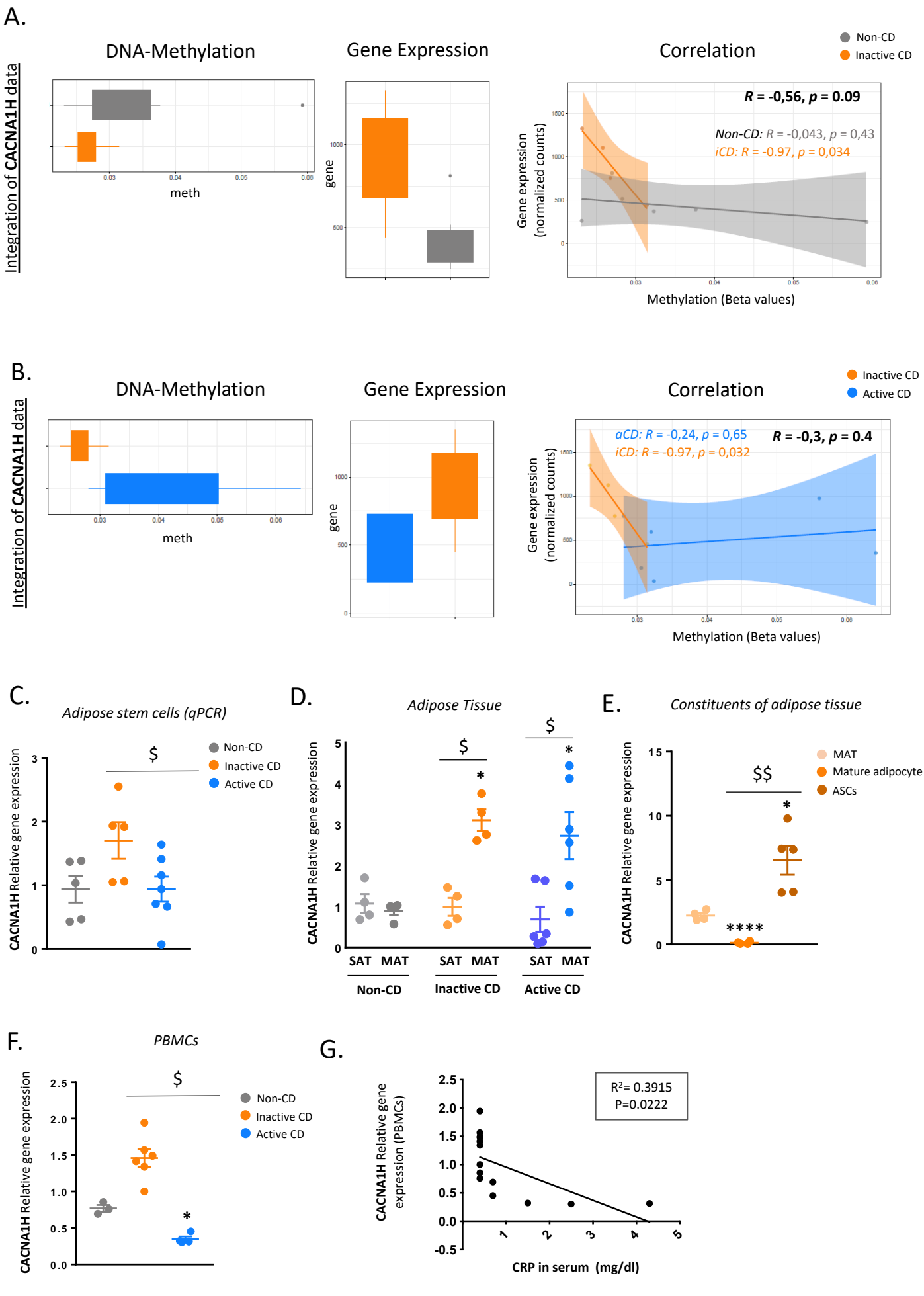
A.
DNA-Methylation
Gene Expression
Correlation
Non-CD
Inactive CD
Integration of CACNA1H data
meth
gene
R = -0,56, p = 0.09
Non-CD: R = -0,043, p = 0,43
iCD: R = -0.97, p = 0,034
Gene expression (normalized counts)
Methylation (Beta values)
B.
DNA-Methylation
Gene Expression
Correlation
Inactive CD
Active CD
Integration of CACNA1H data
meth
gene
aCD: R = -0,24, p = 0,65
iCD: R = -0.97, p = 0,032
R = -0,3, p = 0.4
Gene expression (normalized counts)
Methylation (Beta values)
C.
Adipose stem cells (qPCR)
CACNA1H Relative gene expression
Non-CD
Inactive CD
Active CD
D.
Adipose Tissue
CACNA1H Relative gene expression
SAT MAT
Non-CD
Inactive CD
Active CD
E.
Constituents of adipose tissue
CACNA1H Relative gene expression
MAT
Mature adipocyte
ASCs
F.
PBMCs
CACNA1H Relative gene expression
Non-CD
Inactive CD
Active CD
G.
CACNA1H Relative gene expression (PBMCs)
R²= 0.3915
P=0.0222
CRP in serum (mg/dl)